

CDT—an Entropic Theory of Quantum Gravity

J. Ambjørn, A. Görlich, J. Jurkiewicz and R. Loll

Abstract In these lectures we describe how a theory of quantum gravity may be constructed in terms of a lattice formulation based on so-called causal dynamical triangulations (CDT). We discuss how the continuum limit can be obtained and how to define and measure diffeomorphism-invariant correlators. In four dimensions, which has our main interest, the lattice theory has an infrared limit which can be identified with de Sitter spacetime. We explain why this infrared property of the quantum spacetime is nontrivial and due to “entropic” effects encoded in the nonperturbative path integral measure. This makes the appearance of the de Sitter universe an example of true emergence of classicality from microscopic quantum laws. We also discuss nontrivial aspects of the UV behaviour, and show how to investigate quantum fluctuations around the emergent background geometry. Finally, we consider the connection to the asymptotic safety scenario, and derive from it a new, conjectured scaling relation in CDT quantum gravity.

J. Ambjørn
The Niels Bohr Institute, Blegdamsvej 17, DK-2100 Copenhagen Ø, Denmark ,
e-mail: ambjorn@nbi.dk

A. Görlich
Institute of Physics, Jagellonian University, Reymonta 4, PL 30-059 Krakow, Poland,
e-mail: atg@th.if.uj.edu.pl

J. Jurkiewicz
Institute of Physics, Jagellonian University, Reymonta 4, PL 30-059 Krakow, Poland,
e-mail: jurkiewicz@th.if.uj.edu.pl

R. Loll
Institute for Theoretical Physics, Utrecht University, Leuvenlaan 4, NL-3584 CE Utrecht, The Netherlands, e-mail: r.loll@uu.nl

1 Introduction

How to reconcile the classical theory of general relativity with quantum mechanics remains an unsolved problem. Flat Minkowskian spacetime seems an excellent local approximation to spacetime down to the smallest distances we can probe in the laboratory. At least the Standard Model of elementary particles, which relies heavily on the Minkowskian spacetime structure, works almost too well, leaving us presently with little clue as to what should replace it at shorter spacetime distances, i.e. higher energies. If one naïvely tries to quantize the theory of general relativity by making a perturbative expansion around this flat background one is faced with the fact that the corresponding field theory is not renormalizable. The mass dimension of the gravitational coupling constant is -2 in units where $c = \hbar = 1$. To deal with this problem one can try to go beyond conventional quantum field theory. One such attempt is string theory. However, until now it has added little to our understanding of why to a very good approximation we live in a $3+1$ dimensional classical world governed by Einstein's equations with a positive cosmological constant, around which there presumably are small quantum fluctuations. Loop quantum gravity is another attempt to quantize gravity, which introduces new ways of treating gravity at the Planck scale, but it has problems with recovering classical gravity in the infrared limit. Here we will describe a much more mundane approach using only standard quantum field theory. In a sum-over-histories approach we will attempt to define a nonperturbative quantum field theory which has as its infrared limit ordinary classical general relativity and at the same time has a nontrivial ultraviolet limit. From this point of view it is close in spirit to the renormalization group approach, whose application to gravity with the hope of establishing its *asymptotic safety* was first advocated long ago by Weinberg [1], and more recently substantiated by several groups of researchers [2].

The approach reported here is nontrivial for two reasons which combine to make it genuinely nonperturbative. First of all, as just stated, a theory of quantum gravity is not perturbatively renormalizable, and thus, whatever field theory one invents, it must in some sense be nonperturbative. Here we want to use a lattice to provide an ultraviolet regularization of the quantum field theory. The lattice regularization of quantum field theories has been very successful, but it is usually implemented in flat, Euclidean spacetime, where the Osterwalder-Schrader axioms ensure us that this is unproblematic. One knows how to get from a quantum field theory formulated in Euclidean spacetime to a quantum field theory formulated in Minkowskian spacetime. However, little is known about the analogous issue once we move from flat to curved spacetimes and even more, to a situation where spacetime itself becomes the object of quantization¹. That the situation is nontrivial even at the most elementary level is seen by considering the Einstein-Hilbert action from which we can derive the classical equations of general relativity. It is formally straightforward to rotate this action from Minkowskian to Euclidean signature. However, one then has to face

¹ An extension of the Osterwalder-Schrader axioms to certain diffeomorphism-invariant theories was given in [3].

the fact that the Euclidean action is unbounded below, the unboundedness caused by the “wrong sign” of the conformal mode, corresponding to overall, local rescalings of the metric tensor. This is a potential obstacle for constructing the quantum theory: when trying to sum over all geometries, with weights given by the exponential of minus the action, there are geometries with arbitrarily large negative action which may render the sum over paths ill defined and the Euclidean theory nonsensical. Consequently, the UV lattice regularization of the path integral has to be such that it also regularizes the infinities which can arise due to the conformal factor. Even if such a regularization exists (and it does, as we shall see), how can one ever expect to obtain something finite in the continuum limit where the regularization is supposed to be removed?

The only solution from a continuum point of view is that the correct path integral measure in the Euclidean sector suppresses the unbounded conformal factor. In the lattice approach the measure factor is of an “entropic” nature: it reflects how many configurations (microscopic, geometrical realizations) there are corresponding to a given value of the action. This entropic factor will enter as an integral part of the bare effective lattice action. (We will illustrate this below in toy examples where everything can be calculated analytically.) The “entropy part” of the effective action will be independent of its “bare coupling constant part”. Usually, the possibility of obtaining a continuum limit of a lattice theory is linked to the existence of a critical point (more generally, a critical surface) in coupling constant space. This will also be the case here. The entropy part of the effective action plays a crucial role in determining the critical value of the bare coupling constants, and the continuum quantum field theory will then emerge at that critical point. However, in such cases there may be no “obvious” continuum theory one can read off from the lattice effective action since we might not know the precise form of the entropy part of the effective action. This highlights the truly nonperturbative nature of the continuum theory.

This review article² is organized as follows: first we describe how a two-dimensional toy model of quantum gravity can be solved explicitly, illustrating some of the points made above. Then we describe the four-dimensional theory, the numerical results obtained by Monte Carlo simulations and how to connect the lattice formalism to the renormalization group approach and to a new theory, so-called Hořava-Lifshitz gravity.

2 The CDT formalism in two dimensions

2.1 Generalities

The lattice formulation of *Euclidean* quantum gravity, i.e. the quantum theory of Euclidean geometries, has been very successful in two dimensions. In two dimensions, gravity does not have any field-theoretic degrees of freedom, but neverthe-

² For less technical accounts of this approach to quantum gravity, see [37, 38].

less two-dimensional Euclidean quantum gravity constitutes a nontrivial example of a diffeomorphism-invariant quantum theory of geometries. The lattice theory, regularized by the method of so-called dynamical triangulations (DT), provides a diffeomorphism-invariant cut-off of two-dimensional Euclidean quantum gravity. It is thus a misconception that a lattice regularization will necessarily break diffeomorphism invariance. Rather, one should view the use of DT in the path integral as a way to sum directly over *geometries*, thus avoiding completely the issue of diffeomorphism invariance. The reason why such an interpretation is possible is that the triangulations used in DT can be viewed as piecewise linear geometries without any specific metric assigned to them: once we know the lengths of the links and the gluing of the simplices, we have the complete information about the geometry. Using identical simplices the basic information about the geometry is entirely encoded in the way the simplices are glued together, and the summation over geometries becomes the summation over possible abstract triangulations. The UV cut-off is the length a of the sides of the simplices. Using this formalism, one can formulate a Euclidean theory of quantum gravity using as building blocks Euclidean equilateral simplices and one obtains a lattice version of two-dimensional quantum gravity. It can be solved analytically for finite a and agrees with a continuum quantization of two-dimensional *Euclidean* gravity (quantum Liouville theory) in the limit $a \rightarrow 0$.

However, in spacetime dimension larger than two this Euclidean lattice approach does not seem to have the desired continuum limit. This apparent failure was a key motivation for introducing a modified approach based on so-called causal dynamical triangulations (CDT). It realizes, in a nonperturbative context, ideas put forward in earlier work [4], which advocated that in a gravitational path integral with the correct, Lorentzian signature of spacetime one should sum over causal geometries only.

2.2 The combinatorial solution in two dimensions

Let us describe the explicit solution of CDT in two dimensions, that is, one space and one time dimension [7].

The model is defined as follows. The topology of the underlying manifold is taken to be $S^1 \times [0, 1]$, with “space” represented by the closed manifold S^1 . We consider the evolution of this space in “time”. No topology change of space is allowed.

The geometry of each spatial slice is uniquely characterized by the length assigned to it. In the discretized version, the length L will be quantized in units of a lattice spacing a , i.e. $L = l \cdot a$ where l is an integer. A slice will thus be defined by l vertices and l links connecting them. To obtain a 2d geometry, we will evolve this spatial loop in discrete steps. This leads to a preferred notion of (discrete) “time” t , where each loop represents a slice of constant t . The propagation from time-slice t to time-slice $t + 1$ is governed by the following rule: each vertex i at time t is connected to k_i vertices at time $t + 1$, $k_i \geq 1$, by links which are assigned a “time-like” squared edge length $-a^2$. The k_i vertices, $k_i > 1$, at time-slice $t + 1$ will be

connected by $k_i - 1$ consecutive space-like links, thus forming $k_i - 1$ triangles. Finally the right boundary vertex in the set of k_i vertices will be identified with the left boundary vertex of the set of k_{i+1} vertices. In this way we get a total of $\sum_{i=1}^l (k_i - 1)$ vertices (and also links) at time-slice $t + 1$ and the two spatial slices are connected by $\sum_{i=1}^l k_i \equiv l_t + l_{t+1}$ triangles, see Fig. 1.

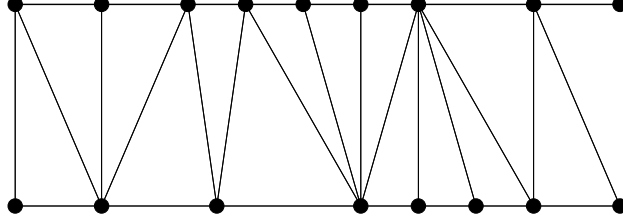


Fig. 1 The propagation of a spatial slice from time step t to step $t + 1$ in two-dimensional causal triangulations. The ends of the strip should be joined to form a band with topology $S^1 \times [0, 1]$.

The elementary building blocks of a geometry are therefore triangles with one space- and two time-like edges. We define them to be flat in the interior. A consistent way of assigning interior angles to such Minkowskian triangles is described in [5]. The angle between two time-like edges is $\gamma_{tt} = -\arccos \frac{3}{2}$, and between a space- and a time-like edge $\gamma_{st} = \frac{\pi}{2} + \frac{1}{2} \arccos \frac{3}{2}$, summing up to $\gamma_{tt} + 2\gamma_{st} = \pi$. The sum over all angles around a vertex with j incoming and k outgoing time-like edges (by definition $j, k \geq 1$) is given by $2\pi + (4 - j - k) \arccos \frac{3}{2}$. The regular triangulation of flat Minkowski space corresponds to $j = k = 2$ at all vertices. The volume of a single triangle is given by $\frac{\sqrt{5}}{4} a^2$.

One may view these geometries as a subclass of all possible triangulations that allow for the introduction of a causal structure. Namely, if we think of all time-like links as being future-directed, a vertex v' lies in the future of a vertex v iff there is an oriented sequence of time-like links leading from v to v' . Two arbitrary vertices may or may not be causally related in this way.

In quantum gravity one sums over all geometries connecting, say, two spatial boundaries of length L_1 and L_2 , with the weight of each geometry g given by

$$e^{iS[g]}, \quad S[g] = \Lambda_0 \int \sqrt{-g} \quad (\text{in 2d}), \quad (1)$$

where Λ_0 is the bare cosmological constant. If in the discretized model we have a piecewise linear geometry made from n triangles the corresponding action will be

$$S = \Lambda_0 \frac{\sqrt{5}a^2}{4} n = \lambda n, \quad \lambda \equiv \Lambda_0 \frac{\sqrt{5}a^2}{4}. \quad (2)$$

In our discretized model the boundaries will be characterized by integers l_1 and l_2 , the number of vertices or links at the two boundaries. The path integral amplitude for the “propagation” from geometry l_1 to l_2 will be the sum over all interpolating

surfaces of the kind described above, with a weight given by the discretized version of (1). Let us call the corresponding amplitude $G_\lambda^{(1)}(l_1, l_2)$. Thus we have

$$G_\lambda^{(1)}(l_1, l_2) = \sum_{t=1}^{\infty} G_\lambda^{(1)}(l_1, l_2; t), \quad (3)$$

$$G_\lambda^{(1)}(l_1, l_2; t) = \sum_{l=1}^{\infty} G_\lambda^{(1)}(l_1, l; 1) l G_\lambda^{(1)}(l, l_2; t-1), \quad (4)$$

$$G_\lambda^{(1)}(l_1, l_2; 1) = \frac{1}{l_1} \sum_{\{k_1, \dots, k_{l_1}\}} e^{i\lambda \sum_{i=1}^{l_1} k_i}, \quad (5)$$

where λ denotes the *bare* dimensionless lattice cosmological constant³ defined in (2), and where t denotes the total number of time-slices connecting l_1 and l_2 .

From a combinatorial point of view it is convenient to mark a vertex on the entrance loop in order to get rid of the factors l and $1/l$ in (4) and (5), that is,

$$G_\lambda(l_1, l_2; t) \equiv l_1 G_\lambda^{(1)}(l_1, l_2; t). \quad (6)$$

(The unmarking of a point may be thought of as the factoring out by (discrete) spatial diffeomorphisms). Note that $G_\lambda(l_1, l_2; 1)$ plays the role of a transfer matrix, satisfying

$$G_\lambda(l_1, l_2; t_1 + t_2) = \sum_l G_\lambda(l_1, l; t_1) G_\lambda(l, l_2; t_2) \quad (7)$$

$$G_\lambda(l_1, l_2; t+1) = \sum_l G_\lambda(l_1, l; 1) G_\lambda(l, l_2; t). \quad (8)$$

Knowing $G_\lambda(l_1, l_2; 1)$ allows us to find $G_\lambda(l_1, l_2; t)$ by iterating (8) t times. This program is conveniently carried out by introducing the generating function for the numbers $G_\lambda(l_1, l_2; t)$,

$$G_\lambda(x, y; t) \equiv \sum_{k, l} x^k y^l G_\lambda(k, l; t), \quad (9)$$

which we can use to rewrite (7) as

$$G_\lambda(x, y; t_1 + t_2) = \oint \frac{dz}{2\pi iz} G_\lambda(x, z^{-1}; t_1) G_\lambda(z, y; t_2), \quad (10)$$

where the contour should be chosen to include the singularities in the complex z -plane of $G_\lambda(x, z^{-1}; t_1)$ but not those of $G_\lambda(z, y; t_2)$.

One can either view the introduction of $G_\lambda(x, y; t)$ as a purely technical device or take x and y as related to boundary cosmological constants. Let λ_i and λ_f denote dimensionless lattice boundary cosmological constants, such that if the entrance

³ One obtains the renormalized (continuum) cosmological constant Λ by an additive renormalization, see below.

boundary consists of k links the lattice boundary action will be $\lambda_i k$, or, introducing a dimensionful bare lattice boundary cosmological constant $\Lambda_i = \lambda_i/a$ and a continuum boundary length $L_i = k a$, $\Lambda_i L_i$ (and similarly $\Lambda_0 = \lambda_0/a$ etc.). We now write

$$x = e^{i\lambda_i} = e^{i\Lambda_i a}, \quad y = e^{i\lambda_f} = e^{i\Lambda_0 a}, \quad (11)$$

such that $x^k = e^{i\lambda_i k}$ becomes the exponential of the boundary cosmological term, and similarly for $y^l = e^{i\lambda_f l}$. Let us for notational convenience define

$$g = e^{i\lambda}. \quad (12)$$

For the technical purpose of counting we view x, y and g as variables in the complex plane. In general the function

$$G(x, y; g; t) \equiv G_\lambda(x, y; t) \quad (13)$$

will be analytic in a neighbourhood of $(x, y, g) = (0, 0, 0)$.

From the definitions (5) and (6) it follows by standard techniques of generating functions that we may associate a factor g with each triangle, a factor x with each vertex on the entrance loop and a factor y with each vertex on the exit loop, leading to

$$G(x, y; g; 1) = \sum_{k=0}^{\infty} \left(gx \sum_{l=0}^{\infty} (gy)^l \right)^k - \sum_{k=0}^{\infty} (gx)^k = \frac{g^2 xy}{(1-gx)(1-gx-gy)}. \quad (14)$$

Formula (14) is simply a book-keeping device for all possible ways of evolving from an entrance loop of any length in one step to an exit loop of any length. The subtraction of the term $1/(1-gx)$ has been performed to exclude the degenerate cases where either the entrance or the exit loop is of length zero.

From (14) and eq. (10), with $t_1 = 1$, we obtain

$$G(x, y; g; t) = \frac{gx}{1-gx} G\left(\frac{g}{1-gx}, y; g; t-1\right). \quad (15)$$

This equation can be iterated and the solution written as

$$G(x, y; g; t) = F_1^2(x) F_2^2(x) \cdots F_{t-1}^2(x) \frac{g^2 xy}{[1-gF_{t-1}(x)][1-gF_{t-1}(x)-gy]}, \quad (16)$$

where $F_t(x)$ is defined iteratively by

$$F_t(x) = \frac{g}{1-gF_{t-1}(x)}, \quad F_0(x) = x. \quad (17)$$

Let F denote the fixed point of this iterative equation. By standard techniques one readily obtains

$$F_t(x) = F \frac{1 - xF + F^{2t-1}(x-F)}{1 - xF + F^{2t+1}(x-F)}, \quad F = \frac{1 - \sqrt{1-4g^2}}{2g}. \quad (18)$$

Inserting (18) in eq. (16), we can write

$$G(x, y; g, t) = \frac{F^{2t}(1-F^2)^2 xy}{(A_t - B_t x)(A_t - B_t(x+y) + C_t xy)} \quad (19)$$

$$= \frac{F^{2t}(1-F^2)^2 xy}{\left[(1-xF) - F^{2t+1}(F-x) \right] \left[(1-xF)(1-yF) - F^{2t}(F-x)(F-y) \right]}, \quad (20)$$

where the time-dependent coefficients are given by

$$A_t = 1 - F^{2t+2}, \quad B_t = F(1 - F^{2t}), \quad C_t = F^2(1 - F^{2t-2}). \quad (21)$$

The combined region of convergence to the expansion in powers $g^k x^l y^m$, valid for all t is

$$|g| < \frac{1}{2}, \quad |x| < 1, \quad |y| < 1. \quad (22)$$

The asymmetry between x and y in the expressions (19) and (20) is due to the marking of the entrance loop. If we also mark the exit loop we have to multiply $G_\lambda(l_1, l_2; t)$ by l_2 . We define

$$G_\lambda^{(2)}(l_1, l_2; t) \equiv l_2 G_\lambda(l_1, l_2; t) = l_1 l_2 G_\lambda^{(1)}(l_1, l_2; t). \quad (23)$$

The corresponding generating function $G^{(2)}(x, y; g; t)$ is obtained from $G(x, y; g; t)$ by acting with $y \frac{d}{dy}$,

$$G^{(2)}(x, y; g; t) = \frac{F^{2t}(1-F^2)^2 xy}{(A_t - B_t(x+y) + C_t xy)^2}. \quad (24)$$

We can compute $G_\lambda(l_1, l_2; t)$ from $G(x, y; g; t)$ by a (discrete) inverse Laplace transformation

$$G_\lambda(l_1, l_2; t) = \oint \frac{dx}{2\pi i x} \oint \frac{dy}{2\pi i y} \frac{1}{x^{l_1}} \frac{1}{y^{l_2}} G(x, y; g; t), \quad (25)$$

where the contours should be chosen in the region where $G(x, y; g; t)$ is analytic. A more straightforward method is to rewrite the right-hand side of (19) as a power series in x and y , yielding

$$G_\lambda(l_1, l_2; t) = \frac{F^{2t}(1-F^2)^2 B^{l_1+l_2}}{l_2 A^{l_1+l_2+2}} \sum_{k=0}^{\min(l_1, l_2)-1} \frac{l_1+l_2-k-1}{k!(l_1-k-1)!(l_2-k-1)!} \left(\frac{A_t C_t}{B_t^2} \right)^k, \quad (26)$$

which, as expected, is symmetric with respect to l_1 and l_2 after division by l_1 .

In the next section we will give explicit expressions for $G_\lambda(l_1, l_2; t)$, $G_\lambda(l_1, l_2)$ and $G_\lambda(x, y)$ (the integral of $G_\lambda(x, y; t)$ over t) in a certain continuum limit.

2.3 The continuum limit

The path integral formalism we are using here is very similar to the one used to represent the free particle as a sum over paths. Also there one performs a summation over geometric objects (the paths), and the path integral itself serves as the propagator. From the particle case it is known that the bare mass undergoes an additive renormalization (even for the free particle), and that the bare propagator is subject to a wave-function renormalization (see [6] for a review). The same is true in two-dimensional gravity, treated in the formalism of dynamical triangulations [6]. The coupling constants with positive mass dimension, i.e. the cosmological constant and the boundary cosmological constants, undergo an additive renormalization, while the partition function itself (i.e. the Hartle-Hawking-like wave functions) undergoes a multiplicative wave-function renormalization. We therefore expect the bare coupling constants λ , λ_i and λ_0 to behave as

$$\frac{\sqrt{5}}{4}\Lambda_0 \equiv \frac{\lambda}{a^2} = \frac{C_\lambda}{a^2} + \tilde{\Lambda}, \quad \Lambda_i \equiv \frac{\lambda_i}{a} = \frac{C_{\lambda_i}}{a} + \tilde{X}, \quad \Lambda_o \equiv \frac{\lambda_f}{a} = \frac{C_{\lambda_f}}{a} + \tilde{Y}, \quad (27)$$

where $\tilde{\Lambda}, \tilde{X}, \tilde{Y}$ denote the renormalized cosmological and boundary cosmological constants and where we have absorbed a factor $\sqrt{5}/4$ in the definition of $\tilde{\Lambda}$.

If we introduce the notation

$$g_c = e^{iC_\lambda}, \quad x_c = e^{iC_{\lambda_i}}, \quad y_c = e^{iC_{\lambda_f}}, \quad (28)$$

for critical values of the coupling constants, it follows from (11) and (12) that

$$g = g_c e^{ia^2\tilde{\Lambda}}, \quad x = x_c e^{ia\tilde{X}}, \quad y = y_c e^{ia\tilde{Y}}. \quad (29)$$

The wave-function renormalization will appear as a multiplicative cut-off dependent factor in front of the bare ‘‘Green’s function’’ $G(x, y; g; t)$,

$$G_{\tilde{\Lambda}}(\tilde{X}, \tilde{Y}; T) = \lim_{a \rightarrow 0} a^\eta G(x, y; g; t), \quad (30)$$

where $T = at$, and where the critical exponent η should be chosen such that the right-hand side of eq. (30) exists. In general this will only be possible for particular choices of g_c , x_c and y_c in (30).

The basic relation (7) can survive the limit (30) only if $\eta = 1$, since we have assumed that the boundary lengths L_1 and L_2 have canonical dimensions and satisfy $L_i = a l_i$.

From eqs. (19) and (21) it is clear that we can only obtain a nontrivial continuum limit if $|F| \rightarrow 1$. This leads to a one-parameter family of possible choices

$$g_c = \frac{1}{2 \cos \alpha} \quad \text{for } F = e^{i\alpha}, \quad \alpha \in \mathbb{R}, \quad (31)$$

for critical values of g . It follows from (12) that most values of g_c correspond to a complex *bare* cosmological constant λ . However, the renormalized cosmological constant $\tilde{\Lambda}$ in (27) (depending on how we approach g_c in the complex plane) could in principle still be real.

A closer analysis reveals that only at $g_c = \pm 1/2$, corresponding to $\alpha = 0, \pi$, is there any possibility of obtaining an interesting continuum limit. Note that these two values are the only ones which can be reached from a region of convergence of $G(x, y; g; t)$ (see Fig. 2). Note also that requiring the bare λ to lie inside the region

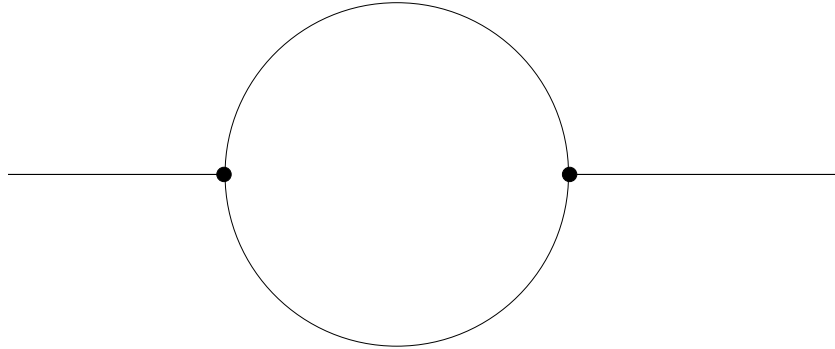


Fig. 2 The circle of convergence in the complex g plane (radius $1/2$), and the critical lines, ending in $g = \pm 1/2$.

of convergence when $g \rightarrow g_c$ leads to a restriction $\text{Im} \tilde{\Lambda} > 0$ on the *renormalized* cosmological constant $\tilde{\Lambda}$, since $|g| < \frac{1}{2} \Rightarrow \text{Im} \lambda > \ln 2$.

Without loss of generality, we will consider the critical value $g_c = 1/2$. It corresponds to a purely imaginary bare cosmological constant $\lambda_c := C_\lambda/a^2 = -i \ln 2/a^2$. If we want to approach this point from the region in the complex g -plane where $G(x, y; g; t)$ converges it is natural to choose the renormalized coupling $\tilde{\Lambda}$ imaginary as well, $\tilde{\Lambda} = i\Lambda$, i.e.

$$\lambda = i \frac{\ln \frac{1}{2}}{a^2} + i\Lambda. \quad (32)$$

One obtains a well-defined scaling limit (corresponding to $\Lambda \in \mathbb{R}$) by letting $\lambda \rightarrow \lambda_c$ along the imaginary axis. The Lorentzian form for the continuum propagator is obtained by an analytic continuation $\Lambda \rightarrow -i\Lambda$ in the *renormalized* coupling of the resulting Euclidean expressions.

At this stage it may seem that we are surreptitiously reverting to a fully Euclidean model. We could of course equivalently have conducted the entire discussion up to this point in the “Euclidean sector”, by omitting the factor of $-i$ in the exponential (1) of the action, choosing λ positive real and taking all edge lengths equal to 1. However, from a purely Euclidean point of view there would not have been any

reason for restricting the state sum to a subclass of geometries admitting a causal structure. The associated preferred notion of a discrete time allows us to define an “analytic continuation in time” (we will discuss this in more detail later for higher-dimensional gravity). Because of the simple form of the action in two dimensions, the rotation

$$\int dx dt \sqrt{-g_{lor}} \rightarrow i \int dx dt_{eu} \sqrt{g_{eu}} \quad (33)$$

to Euclidean metrics in our model is equivalent to the analytic continuation of the cosmological constant Λ . What is special about the above situation is that we perform the analytic continuation configuration by configuration, i.e. geometry by geometry. That is possible because of the particular set of causal geometries we have chosen to include in the regularized path integral. Moreover, as will be clear later, it is a feature which extends to higher dimensions too: each piecewise linear geometry with Lorentzian signature we use in the path integral has an analytic continuation to a Euclidean piecewise linear geometry *and* one has a relation like (33) for the Einstein-Hilbert actions of the two geometries (see later for details).

From (19) or (20) it follows that we can only get macroscopic loops in the limit $a \rightarrow 0$ if we simultaneously take $x, y \rightarrow 1$. (For $g_c = -1/2$, one needs to take $x, y \rightarrow -1$. The continuum expressions one obtains are identical to those for $g_c = 1/2$.) Again the critical points correspond to purely imaginary bare boundary cosmological coupling constants. We will allow for such imaginary couplings and thus approach the critical point $\lambda_i = \lambda_f = 0$ from the region of convergence of $G(x, y; g; t)$, i.e. via real, positive X, Y where

$$\lambda_i = iXa, \quad \lambda_f = iYa. \quad (34)$$

Again X and Y have an obvious interpretation as positive boundary cosmological constants in a Euclidean theory, which may be analytically continued to imaginary values to reach the Lorentzian sector.

Summarizing, we have

$$g = \frac{1}{2} e^{-\Lambda a^2} \rightarrow \frac{1}{2} \left(1 - \frac{1}{2} \Lambda a^2\right), \quad (\text{i.e. } F = 1 - a\sqrt{\Lambda}) \quad (35)$$

as well as

$$x = e^{-Xa} \rightarrow 1 - aX, \quad y = e^{-aY} \rightarrow 1 - aY, \quad (36)$$

where the arrows \rightarrow in (35) and (36) should be viewed as analytic coupling constant redefinitions of Λ, X and Y , which we have performed to get rid of factors of $1/2$ etc. in the formulas below. With the definitions (35) and (36) it is straightforward to perform the continuum limit of $G(x, y; g; t)$ as $(x, y, g) \rightarrow (x_c, y_c, g_c) = (1, 1, 1/2)$, yielding

$$G_\Lambda(X, Y; T) = \frac{4\Lambda e^{-2\sqrt{\Lambda}T}}{(\sqrt{\Lambda} + X) + e^{-2\sqrt{\Lambda}T}(\sqrt{\Lambda} - X)}$$

$$\times \frac{1}{(\sqrt{\Lambda} + X)(\sqrt{\Lambda} + Y) - e^{-2\sqrt{\Lambda}T}(\sqrt{\Lambda} - X)(\sqrt{\Lambda} - Y)}. \quad (37)$$

For $T \rightarrow \infty$ one finds

$$G_\Lambda(X, Y; T) \xrightarrow{T \rightarrow \infty} \frac{4\Lambda e^{-2\sqrt{\Lambda}T}}{(X + \sqrt{\Lambda})^2(Y + \sqrt{\Lambda})}. \quad (38)$$

From $G_\Lambda(X, Y; T)$ we can finally calculate $G_\Lambda(L_1, L_2; T)$, the continuum amplitude for propagation from a loop of length L_1 , with one marked point, at time-slice $T = 0$ to a loop of length L_2 at time-slice T , by an inverse Laplace transformation,

$$G_\Lambda(L_1, L_2; T) = \int_{-i\infty}^{i\infty} dX \int_{-i\infty}^{i\infty} dY e^{XL_1} e^{YL_2} G_\Lambda(X, Y; T). \quad (39)$$

This transformation can be viewed as the limit of (25) for $a \rightarrow 0$. The continuum version of (10) thus reads

$$G_\Lambda(X, Y; T_1 + T_2) = \int_{-i\infty}^{i\infty} dZ G_\Lambda(X, -Z; T_1) G_\Lambda(Z, Y; T_2), \quad (40)$$

where it is understood that the complex contour of integration should be chosen to the left of singularities of $G_\Lambda(X, -Z; T_1)$, but to the right of those of $G_\Lambda(Z, Y; T_2)$. By an inverse Laplace transformation we get in the limit $T \rightarrow \infty$

$$G_\Lambda(L_1, L_2; T) \xrightarrow{T \rightarrow \infty} 4L_1 e^{-\sqrt{\Lambda}(L_1+L_2)} e^{-2\sqrt{\Lambda}T}, \quad (41)$$

where the origin of the factor L_1 is the marking of a point in the entrance loop. For $T \rightarrow 0$ we obtain

$$G_\Lambda(X, Y; T) \xrightarrow{T \rightarrow 0} \frac{1}{X + Y}, \quad (42)$$

in agreement with the expectation that the inverse Laplace transform should behave like

$$G_\Lambda(L_1, L_2; T) \xrightarrow{T \rightarrow 0} \delta(L_1 - L_2). \quad (43)$$

The general expression for $G_\Lambda(L_1, L_2; T)$ can be computed as the inverse Laplace transform of formula (37), yielding

$$G_\Lambda(L_1, L_2; T) = \frac{e^{-[\coth \sqrt{\Lambda}T]\sqrt{\Lambda}(L_1+L_2)}}{\sinh \sqrt{\Lambda}T} \frac{\sqrt{\Lambda L_1 L_2}}{L_2} I_1 \left(\frac{2\sqrt{\Lambda L_1 L_2}}{\sinh \sqrt{\Lambda}T} \right), \quad (44)$$

where $I_1(x)$ is a modified Bessel function of the first kind. The asymmetry between L_1 and L_2 arises because the entrance loop has a marked point, whereas the exit loop has not. The amplitude with both loops marked is obtained by multiplying with L_2 , while the amplitude with no marked loops is obtained after dividing (44) by L_1 . The highly nontrivial expression (44) agrees with the loop propagator obtained

from a bona-fide continuum calculation in proper-time gauge of pure 2d gravity by Nakayama [33].

The important point we want to emphasize here is that the additive renormalization of the cosmological constant is an entropic effect when calculated after rotation to Euclidean signature. In fact, we can write the propagator (13) as

$$G(x, y, g; t) = \sum_{k, l, n} x^k y^l g^n \sum_{T(k, l, n)} \frac{1}{C(T)}, \quad (45)$$

where the summation is over all *causal* triangulations $T(k, l, n)$ (as defined above and rotated to Euclidean signature), consisting of n triangles and with the two boundaries made of k and l links. $C(T)$ is the order of the so-called automorphism group of graph T and in our case, with a mark on one boundary, $C(T) = 1$. The critical point is $g_c = 1/2$. That can only be the case because the number of (causal) triangulations constructed from n triangles grows exponentially as $e^{n \ln 2}$. The continuum renormalized cosmological constant, as defined by eq. (35), emerges when taking the difference between the value of the action for a geometry made of n triangles and the *entropy* of the configurations with a given action (which in this case is proportional to the number of triangles n). More precisely, let the number of causal triangulations which can be constructed from n triangles be

$$\mathcal{N}(n) = f(n) e^{\lambda_c n}, \quad \lambda_c = \ln 2, \quad (46)$$

where $f(n)$ is a prefactor growing slower than exponentially, and which can also depend on the boundary cosmological constants x, y , a dependence we will suppress here. We can now write eq. (45) as

$$G(\lambda) = \sum_n f(n) e^{-(\lambda - \lambda_c)n}, \quad g \equiv e^{-\lambda}. \quad (47)$$

Introducing the notation $A = na^2$ for the continuum area (again disposing of a factor $\sqrt{5}/4$ for notational simplicity) we see that (35) can be written as

$$\lambda = \lambda_c + \Lambda a^2, \quad (48)$$

introducing the renormalized cosmological constant Λ . Eq. (47) can now be written as

$$G(\Lambda) = \int_0^\infty dA f(A/a^2) e^{-\Lambda A}, \quad (49)$$

with the continuum action ΛA and the nontrivial physics contained in the function $f(A/a^2)$.

The two-dimensional CDT model can be generalized in a number of ways: one can use different weights and explore the universality of the model [8] and there exists a Hamiltonian formulation [9]. Matter can be coupled to the model [10] and one can weaken the causal constraints [11]. In addition, one can relax the constraint of a bounded geometry [12].

3 Causal dynamical triangulations in four dimensions

3.1 The choice of triangulations

The generalization from two spacetime dimensions to three or four is in principle straightforward [13, 14]. In what follows we will concentrate on the 4d case. We consider spacetimes with the topology $[0, 1] \times S^3$. In principle we can choose any spatial topology, as long as we do not allow it to change during time evolution. Here, for simplicity, we will always take the topology of space to be that of a three-sphere.

Suppose now that we have a foliation of spacetime where “time” is taken to mean proper time. Each time-slice, with the topology of S^3 , is represented by a three-dimensional triangulation. We choose as the set of possible triangulations of S^3 those which can be constructed from gluing together tetrahedra whose links are all of length $a_s = a$, playing the role of lattice spacing and UV cut-off. These tetrahedra are thus building blocks for our curved S^3 -geometries, which we take to be piecewise linear. The curvature of such a piecewise linear geometry is located at the links. A number of tetrahedra will share a link. Each tetrahedron has a dihedral angle associated with that link, and the sum of dihedral angles of the tetrahedra sharing the link would add up to 2π if space was flat around that link. If the dihedral angles add up to something different it signals that the piecewise linear space is not flat. In our case the tetrahedra are all identical with a dihedral angle $\theta_d = \arccos(1/3)$, which implies there is no exact tessellation of flat three-dimensional space using equilateral tetrahedra. However, it is not important for the use we are making of the piecewise linear geometries: we use them in the path integral where we sum over all geometries (of a given, fixed topology). Thus the important question is whether the set of piecewise linear geometries we are using is dense in the set of geometries relevant for the path integral. To answer this question, we need to know the measure on the set of geometries. Presently we do not even have a mathematical characterization of the set of geometries to be used in the path integral (and the path integral has of course not been defined in any mathematical sense). Will the set of relevant geometries be like the set of paths used in the path integral of the particle, i.e. all continuous paths? Will the path integral over geometries include all “continuous” geometries? Because the answer is presently unknown, we will proceed with a straightforward generalization of the class of piecewise straight paths of the particle case and see what we get.

We now connect two neighbouring S^3 -triangulations $T_3(1)$ and $T_3(2)$, associated with two consecutive discrete proper times 1 and 2, and create a four-dimensional, piecewise linear geometry, such that the corresponding four-dimensional “slab” consists of four-simplices, has the topology of $[0, 1] \times S^3$, and has $T_3(1)$ and $T_3(2)$ as its three-dimensional boundaries. The spatial links (and subsimplices) contained in these four-dimensional simplices lie in either $T_3(1)$ or $T_3(2)$, and the remaining links are time-like with proper length squared $a_t^2 = -\alpha a^2$, $\alpha > 0$. Subsimplices which contain at least one time-like link we will call “time-like”. In discrete units, we can say that $T_3(1)$ and $T_3(2)$ are separated by a single step in time direction, correspond-

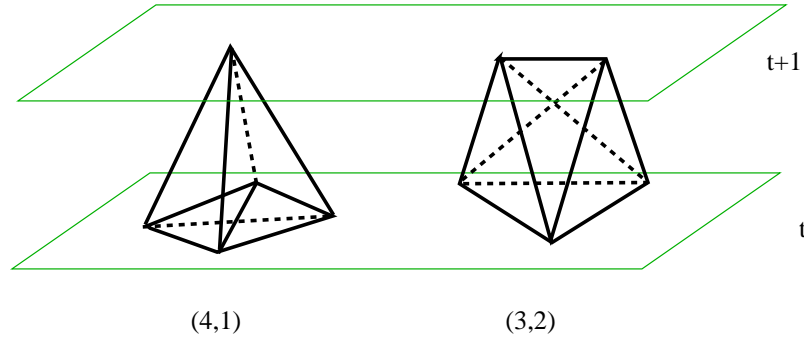


Fig. 3 A (4, 1)- and a (3, 2)-simplex interpolating between two neighbouring spatial slices. The time-reversed (1, 4)- and (2, 3)-simplices are obtained by turning these upside down.

ing to a time-like distance $\sqrt{\alpha}a$ in the sense that each link in the slab which connects the two boundaries has a squared proper length $-\alpha a^2$. It does not imply that all points on the piecewise linear manifold defined by $T_3(1)$ have a proper distance squared $-\alpha a^2$ to the piecewise linear manifold defined by $T_3(2)$ in the piecewise Minkowskian metric of the triangulation.

Thus, our slabs or “sandwiches” are assembled from four-dimensional simplicial building blocks of four kinds, which are labelled according to the number of vertices they share with the two adjacent spatial slices of constant integer proper time. A (4, 1)-simplex has one tetrahedron (and consequently four vertices) in common with $T_3(1)$, and only one vertex in common with $T_3(2)$. It has four time-like links, connecting each of the four vertices in $T_3(1)$ to the vertex belonging to $T_3(2)$. In the second kind of four-simplex, of type (1, 4), the roles of $T_3(1)$ and $T_3(2)$ are interchanged. By contrast, a (3, 2)-simplex has a spatial triangle (and consequently three vertices) in common with the slice $T_3(1)$ and a spatial link (with two vertices) in common with $T_3(2)$, together with six time-like links connecting the two slices. The corresponding (2, 3)-simplex is again obtained by interchanging $T_3(1)$ and $T_3(2)$. The allowed simplices, up to time reversal, are shown in Fig. 3. For our purposes, we need not keep track of the numbers of four-simplices and their time-reversed counterparts separately, and will denote the total number of (4, 1)- and (1, 4)-simplices by $N_4^{(4,1)}$ and similarly the total number of (3, 2)- and (2, 3)-simplices by $N_4^{(3,2)}$. An allowed four-dimensional triangulation of the slab has topology $[0, 1] \times S^3$, is a simplicial manifold with boundary, and is constructed according to the recipe above. To summarize, a path in the gravitational path integral consists of a sequence of triangulations of S^3 , denoted by $T_3(k)$, $k = 0, \dots, n$, where the space between each pair $T_3(k)$ and $T_3(k+1)$ has been filled in by a layer of four-simplices. In the path integral we sum over all possible sequences $\{T_3(k)\}$ and all possible ways of triangulating the slabs in between $T_3(k)$ and $T_3(k+1)$.

3.2 The choice of action

Piecewise linear geometries allow for a natural realization of the Einstein-Hilbert action, as discovered by Regge [15]. For a piecewise linear geometry in d dimensions, defined by a triangulation with length assignments to each link, the curvature is concentrated on the $(d-2)$ -dimensional sub-simplices. For example, in three dimensions the curvature is located at the links, as described above. In dimension four, the curvature is concentrated at the triangles of the triangulation. A direct measure of the sectional curvature of the subspace perpendicular to a given triangle is the *deficit angle* one can associate with it, defined as the difference between the sum of “dihedral” angles of the four-simplices sharing the triangle and 2π . A deficit angle different from zero signifies nonvanishing curvature. In our case we have two kinds of triangles, purely space-like ones and time-like ones (where two of the links are time-like). The local contribution to the total integrated curvature from such a $(d-2)$ -dimensional sub-simplex is the volume of the sub-simplex multiplied by the deficit angle around it, and the integrated discrete (scalar) curvature action is then the sum of these contributions. This leads to a discretized Einstein-Hilbert action of the form

$$\begin{aligned}
S^{\text{EH}} &= \frac{1}{16\pi G} \int d^4x \sqrt{-g(x)} \left(R(x) - 2\Lambda \right) \rightarrow \\
S^{\text{Regge}} &= k \left(\sum_{\substack{\text{space-like} \\ \Delta}} \text{Vol}(\Delta) \frac{1}{i} \left(2\pi - \sum_{\substack{4\text{-simplices} \\ \text{at } \Delta}} \Theta \right) + \sum_{\substack{\text{time-like} \\ \Delta}} \text{Vol}(\Delta) \left(2\pi - \sum_{\substack{4\text{-simplices} \\ \text{at } \Delta}} \Theta \right) \right) \\
&\quad - \lambda \left(\sum_{\substack{(4,1)\&(1,4)\text{-} \\ \text{tetrahedra}}} \text{Vol}(4,1) + \sum_{\substack{(3,2)\&(2,3)\text{-} \\ \text{tetrahedra}}} \text{Vol}(3,2) \right), \tag{50}
\end{aligned}$$

where R is the Ricci scalar curvature and Λ the cosmological constant. Furthermore, we can read off that the constant k is proportional to the inverse of the gravitational coupling constant G and the constant λ is proportional to Λ/G .

It is straightforward to calculate the volumes of the spatial and time-like triangles as well as the four-volumes of the $(4,1)$ - and $(3,2)$ -simplices. This enables us to express the discretized Einstein-Hilbert action as function of the numbers $N_4^{(4,1)}$ and $N^{(3,2)}$ defined in the previous subsection and the total number N_0 of vertices in the triangulation, leading to

$$\begin{aligned}
S^{\text{Regge}} &= (N_0 - \chi) \cdot k\pi\sqrt{4\alpha+1} + \\
&\quad N_4^{(4,1)} \cdot \left(k \frac{\pi}{2} \sqrt{4\alpha+1} - \sqrt{3}k \operatorname{arcsinh} \frac{1}{2\sqrt{2}\sqrt{3\alpha+1}} \right. \\
&\quad \left. - \frac{3k}{2} \sqrt{4\alpha+1} \arccos \frac{2\alpha+1}{2(3\alpha+1)} - \lambda \frac{\sqrt{8\alpha+3}}{96} \right) +
\end{aligned}$$

$$\begin{aligned}
N_4^{(3,2)} \cdot & \left(k\pi\sqrt{4\alpha+1} + \frac{\sqrt{3}k}{4} \operatorname{arcsinh} \frac{\sqrt{3}\sqrt{12\alpha+7}}{2(3\alpha+1)} - \right. \\
& \frac{3k}{4}\sqrt{4\alpha+1} \left(2\arccos \frac{-1}{2\sqrt{2}\sqrt{2\alpha+1}\sqrt{3\alpha+1}} + \arccos \frac{4\alpha+3}{4(2\alpha+1)} \right) \\
& \left. - \lambda \frac{\sqrt{12\alpha+7}}{96} \right). \tag{51}
\end{aligned}$$

For details of the derivation of this formula from (50) we refer to [14]. The quantity χ denotes the Euler characteristic of the four-dimensional spacetime and appears because we have been using the Euler relation $N_0 - N_1 + N_2 - N_3 + N_4 = \chi$ along with other so-called Dehn-Somerville relations to express the numbers N_1, N_2 and N_3 in terms of N_4 and N_0 , where N_i counts the number of i -dimensional (sub-)simplices of a given triangulation. The constant α comes from allowing for a finite scaling $a_t^2 = -\alpha a_s^2$ between the length assignment of the proper length of space- and time-like links.

The Lorentzian action (51) is obviously real for $\alpha > 0$. We now want to study its rotation to Euclidean signature. This is naturally implemented by performing an analytic continuation in α from positive to negative α . In this way, the squared proper lengths of all links become positive and we have a piecewise linear geometry of Euclidean signature, where the links connecting two vertices from neighbouring time slices have length $a_t^2 = |\alpha|a_s^2$. Of course, we also want the Euclideanized four-simplices to be nondegenerate. This requires $-\alpha > 7/12$, the value below which a $(3, 2)$ -simplex becomes degenerate. Performing the analytic continuation in the complex lower α -half-plane and ending at a negative value smaller than $-7/12$ results in the following Euclidean action (*note that we have made a redefinition $\alpha \rightarrow -\alpha$, such that now $\alpha > 7/12$*):

$$\begin{aligned}
S_E^{\text{Regge}} &= -k\pi\sqrt{4\alpha-1}(N_0 - \chi) \\
&+ N_4^{(4,1)} \left(k\sqrt{4\alpha-1} \left(-\frac{\pi}{2} - \frac{\sqrt{3}}{\sqrt{4\alpha-1}} \arcsin \frac{1}{2\sqrt{2}\sqrt{3\alpha-1}} \right. \right. \\
&\quad \left. \left. + \frac{3}{2} \arccos \frac{2\alpha-1}{6\alpha-2} \right) + \lambda \frac{\sqrt{8\alpha-3}}{96} \right) \\
&+ N_4^{(3,2)} \left(k\sqrt{4\alpha-1} \left(-\pi + \frac{\sqrt{3}}{4\sqrt{4\alpha-1}} \arccos \frac{6\alpha-5}{6\alpha-2} + \frac{3}{4} \arccos \frac{4\alpha-3}{8\alpha-4} \right. \right. \\
&\quad \left. \left. + \frac{3}{2} \arccos \frac{1}{2\sqrt{2}\sqrt{2\alpha-1}\sqrt{3\alpha-1}} \right) + \lambda \frac{\sqrt{12\alpha-7}}{96} \right). \tag{52}
\end{aligned}$$

This action is precisely the Regge action for a piecewise linear geometry, constructed from Euclidean building blocks where $a_t^2 = |\alpha|a_s^2$. By analytic continuation in the complex lower-half α -plane we have therefore arrived at the usual formula

$$iS_{Minkowski} \rightarrow -S_{Euclidean} \quad (53)$$

from quantum field theory, where $S_{Euclidean}$ expressed in terms of (continuum) Euclidean geometry is

$$S_E^{EH} = -\frac{1}{16\pi G} \int d^4\xi \sqrt{g(\xi)} \left(R(\xi) - 2\Lambda \right). \quad (54)$$

In quantum field theory on a flat, Minkowskian background such a ‘‘Wick rotation’’ does not usually refer to a specific configuration in the path integral. A configuration will typically not even be differentiable and therefore not have any analytic continuation. Rather, it will refer to the functional form of the action $S[\phi]$ and how it changes by formally replacing it_M by t_E . This reflects the fact that the Feynman propagator, i.e. the result of a functional integration over the field(s) ϕ , has specific analytic properties which allow for a rotation in t to the corresponding Euclidean propagator. In our framework the situation is different, in that each individual piecewise linear geometry can be rotated to a corresponding Euclidean geometry and its associated action transforms in accordance with (53).

For what follows it will be convenient to simplify this action and write it as

$$S_E^{\text{Regge}} = -(\kappa_0 + 6\Delta)N_0 + \kappa_4(N_4^{(4,1)} + N_4^{(3,2)}) + \Delta(2N_4^{(4,1)} + N_4^{(3,2)}), \quad (55)$$

where $\kappa_0 = k\pi\sqrt{4\alpha - 1}$, κ_4 is a linear combination of k and λ with coefficients depending of α , and Δ is, for fixed κ_0 and κ_4 , a function of α , chosen such that for $\alpha = 1$ (i.e. when $a_t = a_s$) we have $\Delta = 0$. For the values of κ_0 and κ_4 which will be of interest for us any $\Delta > 0$ corresponds to $a_t < a_s$. In Fig. 4 we show α as function of Δ for $\kappa_0 = 2.2$ and κ_4 chosen critical (a concept to be discussed shortly). Furthermore, we have dropped the term involving χ . It plays no role in the dynamics since we are not changing the topology.

3.3 The entropic theory of gravity and its phase diagram

Having chosen the cut-off and an action, we can now write down the path integral or partition function for the CDT version of quantum gravity,

$$Z(G, \Lambda) = \int \mathcal{D}[g] e^{-S_E^{EH}[g]} \rightarrow Z(\kappa_0, \kappa_4, \Delta) = \sum_T \frac{1}{C_T} e^{-S_E(T)}, \quad (56)$$

where the summation is over all causal triangulations T of the kind described above, and we have dropped the superscript ‘‘Regge’’ on the discretized action S_E given by (55). Like in the two-dimensional model, the factor $1/C_T$ is a symmetry factor, given by the inverse of the order C_T of the automorphism group of the triangulation T . Note that we can write the partition function as

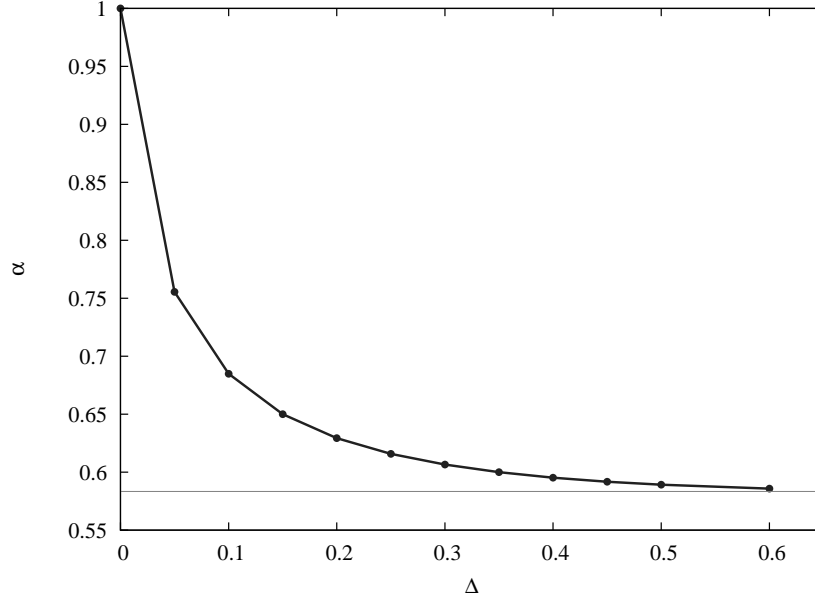


Fig. 4 Plot of the asymmetry factor α , defined as $a_t^2 = \alpha a_s^2$, where a_t and a_s are the lengths of time-like and space-like links, plotted as a function of Δ . The horizontal line is $\alpha = 7/12$, the lowest allowed value of α , where the (3,2)-simplices collapse in the time direction.

$$Z(\kappa_0, \kappa_4, \Delta) = \sum_{N_4, N_4^{(4,1)}, N_0} e^{-(\kappa_4 + \Delta)N_4} e^{-\Delta N_4^{(4,1)}} e^{(\kappa_0 + 6\Delta)N_0} \sum_{T(N_4, N_4^{(4,1)}, N_0)} \frac{1}{C_T}. \quad (57)$$

Introducing

$$x = e^{-(\kappa_4 + \Delta)}, \quad y = e^{-\Delta}, \quad z = e^{(\kappa_0 + 6\Delta)}, \quad (58)$$

we can write

$$\tilde{Z}(x, y, z) = \sum_{N_4, N_4^{(4,1)}, N_0} x^{N_4} y^{N_4^{(4,1)}} z^{N_0} \mathcal{N}(N_4, N_4^{(4,1)}, N_0), \quad (59)$$

where $\mathcal{N}(N_4, N_4^{(4,1)}, N_0)$ denotes the number of CDT configurations with N_4 four-simplices of which $N_4^{(4,1)}$ are of type (4, 1) or (1, 4), and with N_0 vertices, including symmetry factors. Thus the calculation of the partition function is in principle a combinatorial problem, just as in two dimensions where we could solve the problem explicitly (and formula (59) is similar to (45)). This is the reason why we call the model entropic: *the partition function is entirely determined by the number of geometries in the simplest possible way, namely, by being the generating function for these numbers*. The counting of geometric “microscopic” configurations of given $(N_4, N_4^{(4,1)}, N_0)$ is their entropy in the sense of statistical models. Unlike in two di-

mensions, it has until now not been possible to solve this counting problem analytically, which means that we will have to rely on numerical methods.

Let us first understand better the nature of the partition function given by (57). We can write the sum as

$$Z(\kappa_0, \kappa_4, \Delta) = \sum_{N_4} e^{-(\kappa_4 + \Delta)N_4} Z_{N_4}(\kappa_0, \Delta), \quad (60)$$

where $Z_{N_4}(\kappa_0, \Delta)$ is the partition function for a fixed number N_4 of four-simplices, namely,

$$Z_{N_4}(\kappa_0, \Delta) = \sum_{T_{N_4}} \frac{1}{C_T} e^{-\Delta N_4^{(4,1)}(T_{N_4})} e^{(\kappa_0 + 6\Delta)N_0(T_{N_4})}. \quad (61)$$

One can show that $Z_{N_4}(\kappa_0, \Delta)$ is exponentially bounded as a function of N_4 [16],

$$Z_{N_4}(\kappa_0, \Delta) \leq e^{(\kappa_4^c + \Delta)N_4} f(N_4, \kappa_0, \Delta), \quad (62)$$

where $f(N_4)$ grows slower than exponentially. We call κ_4^c the *critical* value of κ_4 . It is a function of Δ and κ_0 and plays the same role as λ_c in the two-dimensional model discussed above: the partition function is only defined for $\kappa_4 > \kappa_4^c$ and the “infinite-volume” limit, where $\langle N_4 \rangle \rightarrow \infty$ can only be achieved for $\kappa_4 \rightarrow \kappa_4^c$. We are interested in sending the lattice spacings $a = a_s, a_t$ to zero while keeping the physical four-volume, which is roughly $N_4 a^4$, fixed. Thus we want to consider the limit $N_4 \rightarrow \infty$, and fine-tune κ_4 to κ_4^c for fixed κ_0, Δ . This fine-tuning is similar to the fine-tuning $\lambda \rightarrow \lambda_c$ in the two-dimensional model. Like there, we expect the *physical* cosmological constant Λ to be defined by the *approach* to the critical point according to

$$\kappa_4 = \kappa_4^c + \frac{\Lambda}{16\pi G} a^4, \quad (63)$$

an equation similar to (48). It ensures that the term

$$(\kappa_4 - \kappa_4^c) N_4 = \frac{\Lambda}{16\pi G} V_4, \quad V_4 = N_4 a^4, \quad (64)$$

gives rise to the standard cosmological term in the Einstein-Hilbert action. The corresponding phase diagram is described qualitatively by Fig. 5. The shaded surface is the “critical surface”, which we want to approach from above (by decreasing κ_4). We put “critical surface” in quotation marks since more correctly fine-tuning to this surface corresponds to taking the limit of infinite four-volume, which does *not necessarily* imply also a continuum limit. The situation here may be different from that of the two-dimensional model, where approaching λ_c automatically meant taking a continuum limit. Two-dimensional quantum gravity is of course a very simple model with no propagating degrees of freedom, whereas in four-dimensional quantum gravity we expect to have genuinely propagating field degrees of freedom. Thus the situation is more like in ordinary Euclidean lattice field theory/critical phenomena, where “infinite volume” does not necessarily mean “continuum limit”.

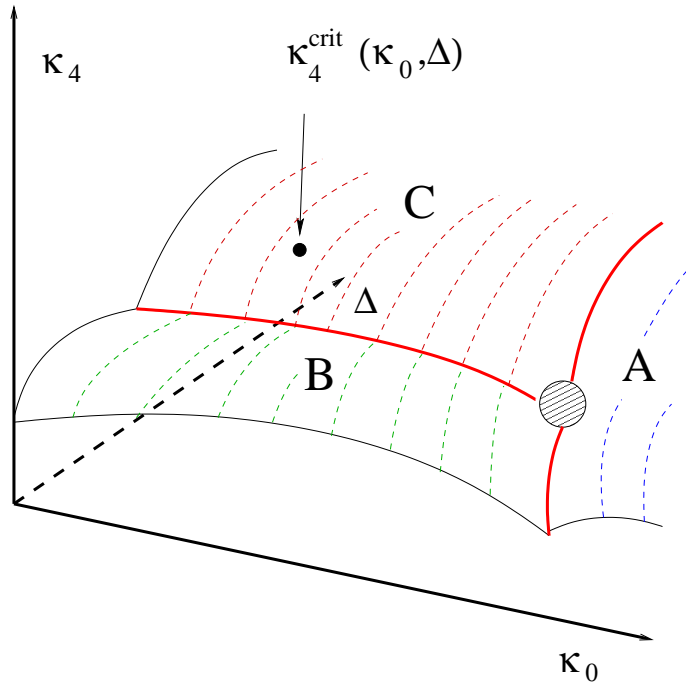


Fig. 5 The phases A, B and C in the coupling constant space spanned by $(\kappa_0, \Delta, \kappa_4)$. Phase C is the one where extended four-dimensional geometries emerge.

A good example of what one might expect is the Ising model on a finite lattice. To obtain a phase transition for this model one has to take the lattice volume to infinity, since there are no genuine phase transitions for finite systems. However, just taking the lattice volume to infinity is not sufficient to ensure critical behaviour of the Ising model. We also have to tune the coupling constant to its critical value, at which point the spin-spin correlation length diverges. Similarly, having placed ourselves on the “critical” surface of CDT quantum gravity or, rather, its “infinite-volume” surface, we can discuss the various phases, indicated in the figure as A, B and C. We move between these phases by changing the bare coupling constants Δ and κ_0 . The solid lines drawn on the surface are the phase transition lines between the (potentially) different phases, which can be of first or higher order. In order to go from the discrete lattice to the continuum theory, we are often interested in a second- or higher-order phase transition, since such transitions are associated with divergent correlation lengths of the field propagators, allowing one to forget about the lattice spacing relative to the correlation length. We will be looking for such transition points.

How can one imagine obtaining an interesting continuum behaviour as a function of κ_0 ? For the purpose of illustration, let us assume that the subleading correction $f(N_4, k_0)$ has the form

$$f(N_4, \kappa_0) = e^{k(\kappa_0)\sqrt{N_4}}, \quad (65)$$

(where later we will check numerically that such a term is indeed present, cf. eq. (78)). The partition function now has the form

$$Z(\kappa_4, \kappa_0) = \sum_{N_4} e^{-(\kappa_4 - \kappa_4^c)N_4 + k(\kappa_0)\sqrt{N_4}}. \quad (66)$$

For dimensional reasons we expect the classical Einstein term in the action to scale like

$$\frac{1}{16\pi G} \int d^4\xi \sqrt{g(\xi)} R(\xi) \propto \frac{\sqrt{V_4}}{G}, \quad (67)$$

motivating the search for a value κ_0^c with $k(\kappa_0^c) = 0$, with the approach to this point governed by

$$k(\kappa_0) \propto \frac{a^2}{G}, \quad \text{i.e.} \quad k(\kappa_0)\sqrt{N_4} \propto \frac{\sqrt{V_4}}{G}. \quad (68)$$

With such a choice we can identify a continuum limit where $\langle N_4 \rangle$, calculated from (66) (by a trivial saddle point calculation), goes to infinity while $a \rightarrow 0$,

$$\langle N_4 \rangle = \frac{\sum_{N_4} N_4 e^{-(\kappa_4 - \kappa_4^c)N_4 + k(\kappa_0)\sqrt{N_4}}}{\sum_{N_4} e^{-(\kappa_4 - \kappa_4^c)N_4 + k(\kappa_0)\sqrt{N_4}}} \approx \frac{k^2(\kappa_0)}{4(\kappa_4 - \kappa_4^c)^2} \propto \frac{1}{\Lambda^2 a^4}. \quad (69)$$

Thus we find

$$\langle V_4 \rangle \propto \frac{1}{\Lambda^2}, \quad Z(\kappa_4, \kappa_0) \approx \exp\left(\frac{k^2(\kappa_0)}{4(\kappa_4 - \kappa_4^c)}\right) = \exp\left(\frac{c}{G\Lambda}\right), \quad (70)$$

as one would naïvely expect from Einstein's equations, with the partition function being dominated by a typical instanton contribution, for a suitable constant c .

The actual set-up for the computer simulations is slightly different from the theoretical framework discussed above, in that we choose to work with a fixed number of four-simplices N_4 in the computer simulations, rather than fine-tuning κ_4 to its critical value. We can perform computer simulations for various N_4 (and fixed κ_0, Δ) and in this way check scaling with respect to N_4 . This is an alternative to fine-tuning κ_4 , and much more convenient from a computational point of view. For large N_4 we can then check whether there are any finite-size effects or whether effectively we already are at the ‘‘critical surface’’ shown in Fig. 5. In addition, we fix the total number N_t of spatial slices, with proper-time labels $t_1, t_2 = t_1 + a_t$, up to $t_{N_t} = t_1 + (N_t - 1)a_t$, where $\Delta t \equiv a_t$ is the discrete lattice spacing in the temporal direction⁴, and denote by $T = N_t a_t$ the total extension of the universe in proper time. For convenience we identify t_{N_t+1} with t_1 , in this way imposing the topology $S^1 \times S^3$ rather than $[0, 1] \times S^3$. This choice does not affect physical results, as will become clear below when we present the numerical results.

⁴ The separation between adjacent slices is a_t , in the sense that all links connecting two neighbouring slices have length a_t , as discussed above.

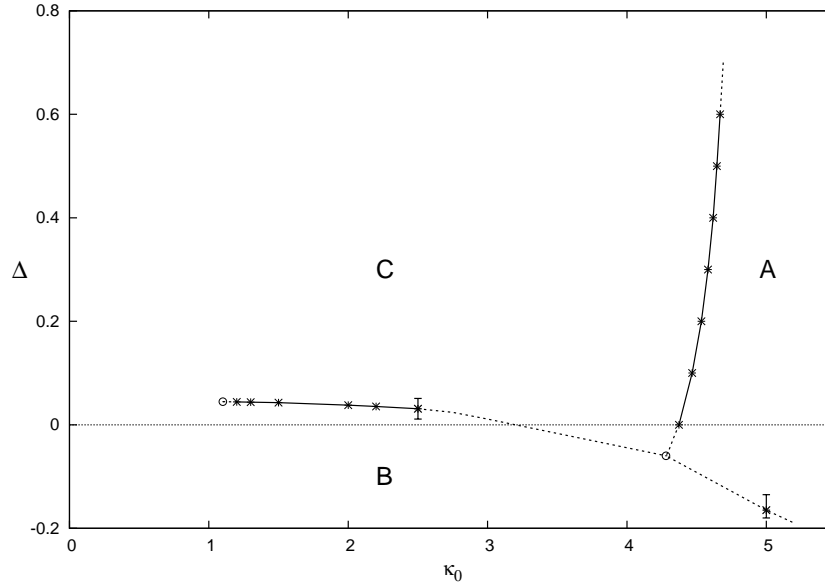


Fig. 6 The phase diagram of four-dimensional quantum gravity, defined in terms of causal dynamical triangulations, parametrized by the inverse bare gravitational coupling κ_0 and the asymmetry parameter Δ .

Finally, the computer simulations are so-called Monte Carlo simulations, where the computer simply generates a sequence of configurations, in this case piecewise linear geometries, with the correct probability distribution, as dictated by the measure and action used in the path integral. It is based on a local updating in terms of “moves”, which change the piecewise linear geometry in a well-defined way (see [14] for a detailed description). These geometries are used to calculate expectation values of observables.

3.4 The actual phase diagram

Based on computer simulations with $N_4 = 80.000$ we have constructed the phase diagram shown in Fig. 6 [23]. The dotted lines in the figure represent mere extrapolations, and lie in a region of coupling constant space which is difficult to access due to the inefficiencies of our computer algorithms.

There are three phases, labeled A, B and C. In phase C, which had our main interest in [18, 19, 21, 20], we observe a genuinely four-dimensional universe in the sense that as a function of the continuum four-volume V_4 (linearly related to the number of four-simplices), the time extent scales as $V_4^{1/4}$ and the spatial volume as

$V_4^{3/4}$. Moving into phase A, these scaling relations break down. Instead, we observe a number of small universes arranged along the time direction like “pearls on a string”, if somewhat uneven in size. Individual beads along the time direction can grow and shrink, be created or disappear as a function of the Monte Carlo time used in the simulations. These small universes are connected by thin “necks”, i.e. slices of constant integer time t_n , where the spatial S^3 -universes are at or close to the smallest three-volume permitted (consisting of five tetrahedra glued together), thus preventing “time” from becoming disconnected.

By contrast, phase B is characterized by the “vanishing” of the time direction, in the sense that only one spatial hypersurface has a three-volume appreciably larger than the minimal cut-off size of five just mentioned. One might be tempted to conclude that the resulting universe is three-dimensional, just lacking the time direction of the extended universe found in phase C. However, the situation is more involved; although we have a large three-volume collected at a single spatial hypersurface, the corresponding spatial universe has almost no extension in the spatial directions. This follows from the fact (ascertained through direct measurement) that it is possible to get in just a few steps from one tetrahedron to any other by moving along the centres of neighbouring tetrahedra or, alternatively, from one vertex to any other along a chain of links. The Hausdorff dimension is therefore quite high, and possibly infinite. Let us assume for the moment that it is indeed infinite; then the universe in phase B has neither time nor spatial extension, and there is no geometry in any classical sense.

We can now give the following qualitative characterization of the three phases in terms of what we will provisionally call “average geometry”. The universe of phase C exhibits a classical four-dimensional background geometry on large scales, such that $\langle geometry \rangle \neq 0$. One may even argue that $\langle geometry \rangle = const.$ in view of the fact that according to the minisuperspace analysis of [20, 21, 36] and allowing for a finite, global rescaling of the renormalized proper time, the universe can be identified with the round S^4 , a maximally symmetric de Sitter space of constant scalar curvature (as we will describe in detail below). By contrast, in phase B the universe presumably has no extension or trace of classicality, corresponding to $\langle geometry \rangle = 0$. Lastly, in phase A, the geometry of the universe appears to be “oscillating” in the time direction. The different behaviour of typical configurations is shown in Fig. 7. The “time” direction is horizontal and we plot the three-volume $N_3(t)$, i.e. the number of tetrahedra in a given time slice, as the circumference of a circle. The three phases are separated by three phase transition lines which meet in a triple point as illustrated in Fig. 6.

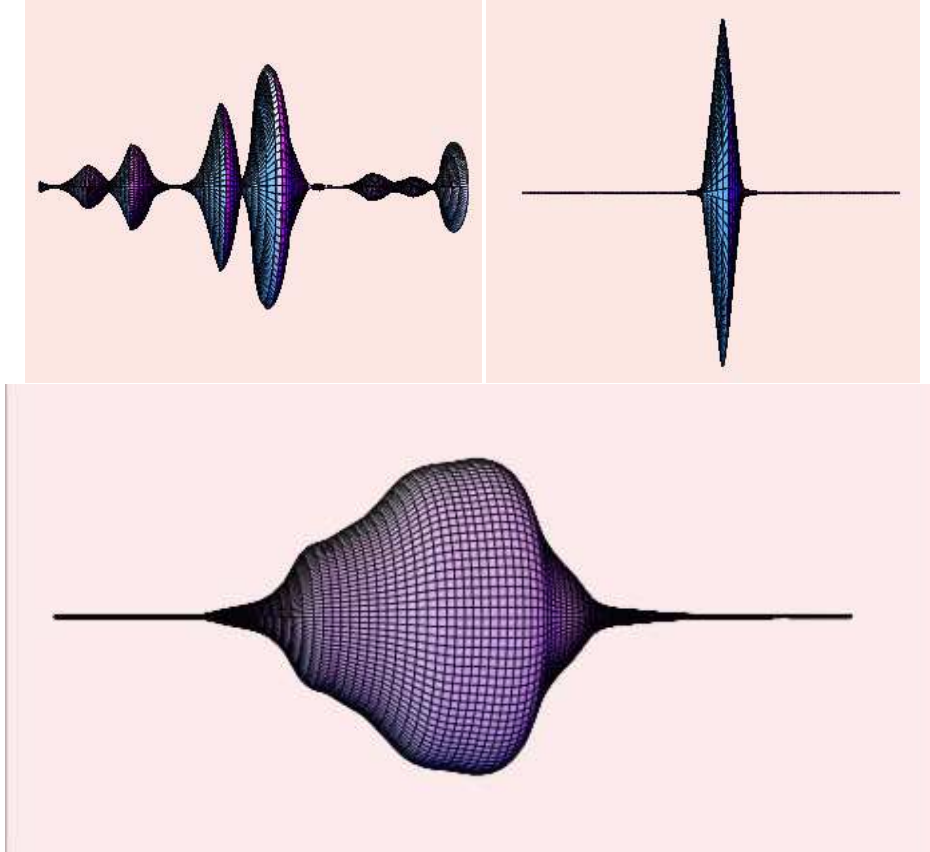


Fig. 7 The volume profiles of typical configurations in the phases A, B and C. Phase C (bottom figure) is the one where extended four-dimensional geometries emerge.

4 The macroscopic de Sitter universe (phase C)

4.1 Identifying the infrared part of the universe

Phase C in the above-mentioned phase diagram has our main interest, because this is where we observe an extended four-dimensional universe. We will now discuss in more detail the geometric properties of this “macroscopic” universe. The measurements reported in this Section have been performed at the values $(\kappa_0, \Delta) = (2.2, 0.6)$ of the bare coupling constants, a point which lies well inside phase C.

The Monte Carlo simulations referred to above will generate a sequence of spacetime histories. An individual spacetime history is not an observable, in the same way as a path $x(t)$ of a particle in the quantum-mechanical path integral is not. However, it is perfectly legitimate to talk about the *expectation value* $\langle x(t) \rangle$ as well as the

fluctuations around $\langle x(t) \rangle$, both of which are in principle calculable in quantum mechanics.

Obviously, there are many more dynamical variables in quantum gravity than there are in the particle case. We can still imitate the quantum-mechanical situation by picking out a particular one, for example, the spatial three-volume $V_3(t)$ at proper time t . We can measure both its expectation value $\langle V_3(t) \rangle$ as well as fluctuations around it. The former gives us information about the large-scale “shape” of the universe we have created in the computer. A “measurement” of $V_3(t)$ consists of a table $N_3(i)$, where $i = 1, \dots, N_t$ and N_t denotes the total number of time slices. The time axis has a total length of N_t time steps, where $N_t = 80$ in the actual simulations, and we have cyclically identified time slice $N_t + 1$ with time slice 1.

What we observe in the simulations is that for the range of discrete volumes N_4 under study the universe does *not* extend (i.e. has appreciable three-volume) over the entire time axis, but rather is localized in a region much shorter than 80 time steps. Outside this region the spatial extension $N_3(i)$ will be minimal, consisting of the minimal number (five) of tetrahedra needed to form a three-sphere S^3 , plus occasionally a few more tetrahedra.⁵ This thin “stalk” therefore carries little four-volume, which means that in a given simulation we can for most practical purposes consider the total four-volume of the remainder, the extended universe, as fixed.

In order to perform a meaningful average over geometries which explicitly refers to the extended part of the universe, we have to remove the translational zero mode present, see [21] for a discussion of the procedure. Having defined the “centre of volume” along the time direction of our spacetime configurations, we can now perform superpositions of configurations and define the average $\langle N_3(i) \rangle$ as a function of the discrete time i . The results of measuring this average discrete spatial size of the universe at various discrete times i are illustrated in Fig. 8 and can be succinctly summarized by the formula

$$N_3^{cl}(i) := \langle N_3(i) \rangle = \frac{N_4}{2(1+\xi)} \frac{3}{4} \frac{1}{s_0 N_4^{1/4}} \cos^3 \left(\frac{i}{s_0 N_4^{1/4}} \right), \quad s_0 \approx 0.59, \quad (71)$$

where $N_3(i)$ denotes the number of three-simplices in the spatial slice at discretized time i and N_4 the total number of four-simplices in the entire universe. ξ is a constant referring to the fact that we have a nonvanishing asymmetry Δ , which implies different lengths for time- and space-like links and consequently different four-volumes for four-simplices of type (4,1) and (3,2). Likewise, the ratio $N_4^{(4,1)}/N_4^{(3,2)}$ depends on the choice of bare coupling constants and has to be measured. Of course, formula (71) is only valid in the extended part of the universe where the spatial three-volumes are larger than the minimal cut-off size.

The data shown in Fig. 8 have been collected at the couplings $(\kappa_0, \Delta) = (2.2, 0.6)$ and for $N_4 = 362.000$. For these particular values of (κ_0, Δ) we have verified relation (71) for N_4 ranging from 45.500 to 362.000 building blocks (45.500, 91.000,

⁵ This kinematic constraint ensures that the triangulation remains a *simplicial manifold* in which, for example, two d -simplices are not allowed to have more than one $(d-1)$ -simplex in common.

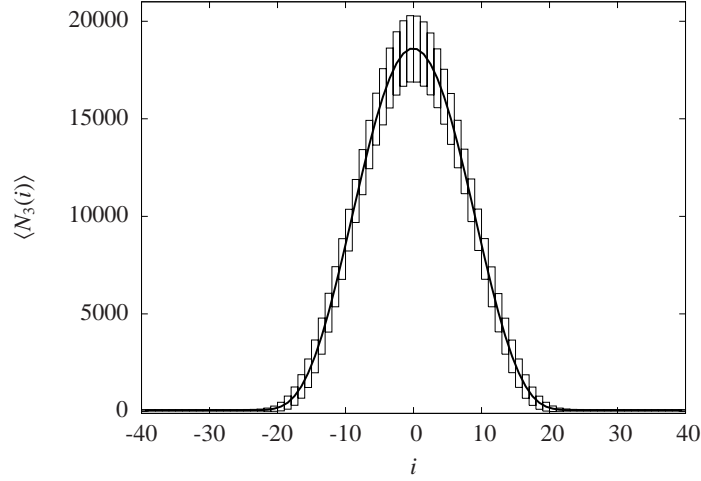


Fig. 8 Background geometry $\langle N_3(i) \rangle$: MC measurements for fixed $N_4 = 362.000$ and best fit (71) yield indistinguishable curves at given plot resolution. The bars indicate the average size of quantum fluctuations.

181.000 and 362.000). After rescaling the time and volume variables by suitable powers of N_4 according to relation (71), and plotting them in the same way as in Fig. 8, one finds almost total agreement between the curves for different spacetime volumes, as illustrated in Fig. 9. This constitutes a beautiful example of finite-size scaling. At least with regard to measuring the average three-volume $V_3(t)$ all our discretized volumes N_4 are sufficiently large to be treated as infinite, in the sense that no further changes will occur for larger N_4 .

By contrast, the quantum fluctuations indicated in Fig. 8 as vertical bars for each discrete time i are volume-dependent and will become (relatively) larger when the total four-volume is decreased. Eq. (71) shows that spatial volumes scale according to $N_4^{3/4}$ and time intervals according to $N_4^{1/4}$, as one would expect for a genuinely *four*-dimensional spacetime. This is exactly the scaling we have used in Fig. 9. It strongly suggests a translation of (71) to a continuum notation. The most natural identification is given by

$$\sqrt{g_{tt}} V_3^{cl}(t) = V_4 \frac{3}{4B} \cos^3\left(\frac{t}{B}\right), \quad (72)$$

where we have made the identifications

$$\frac{t_i}{B} = \frac{i}{s_0 N_4^{1/4}}, \quad \Delta t_i \sqrt{g_{tt}} V_3(t_i) = 2\tilde{C}_4 N_3(i) a^4, \quad (73)$$

such that

$$\int dt \sqrt{g_{tt}} V_3(t) = V_4. \quad (74)$$

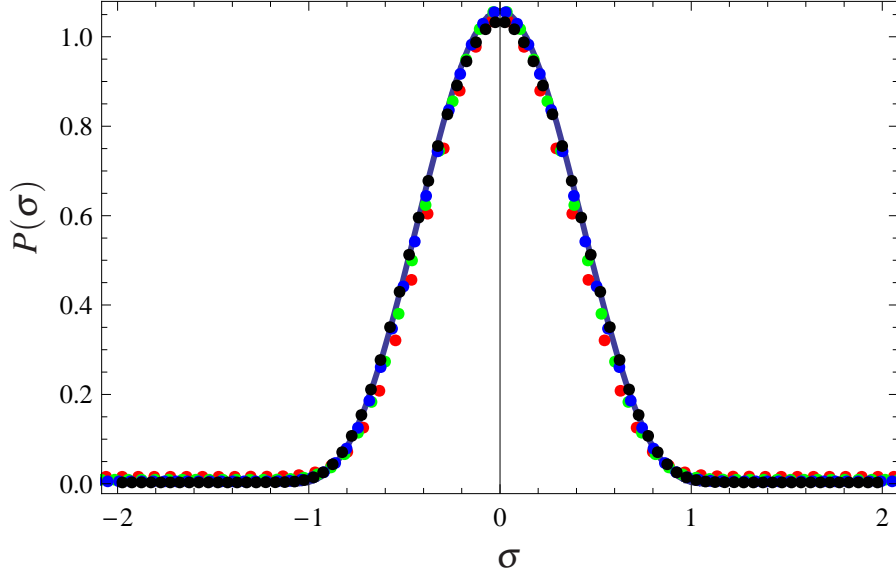


Fig. 9 Rescaling of time and volume variables according to relation (71) for $N_4 = 45.500, 91.000, 181.000$ and 362.000 . The plot also include the curve (71). More precisely: $\sigma \propto i/N_4^{1/4}$ and $P(\sigma) \propto N_3(i)/N_4^{3/4}$.

In (73), $\sqrt{g_{tt}}$ is the constant proportionality factor between the time t and genuine continuum proper time τ , $\tau = \sqrt{g_{tt}} t$. (The combination $\Delta t_i \sqrt{g_{tt}} V_3$ contains \tilde{C}_4 , related to the four-volume of a four-simplex rather than the three-volume corresponding to a tetrahedron, because its time integral must equal V_4). Writing $V_4 = 8\pi^2 R^4/3$, and $\sqrt{g_{tt}} = R/B$, eq. (72) is seen to describe a Euclidean *de Sitter universe* (a four-sphere, the maximally symmetric space for positive cosmological constant) as our searched-for, dynamically generated background geometry! In the parametrization of (72) this is the classical solution to the action

$$S = \frac{1}{24\pi G} \int dt \sqrt{g_{tt}} \left(\frac{g^{tt} \dot{V}_3^2(t)}{V_3(t)} + k_2 V_3^{1/3}(t) - \lambda V_3(t) \right), \quad (75)$$

where $k_2 = 9(2\pi^2)^{2/3}$ and λ is a Lagrange multiplier, fixed by requiring that the total four-volume be V_4 , $\int dt \sqrt{g_{tt}} V_3(t) = V_4$. Up to an overall sign, this is precisely the Einstein-Hilbert action for the scale factor $a(t)$ of a homogeneous, isotropic universe (rewritten in terms of the spatial three-volume $V_3(t) = 2\pi^2 a(t)^3$), although we of course never put any such simplifying symmetry assumptions into the CDT model. The intriguing possibility of describing the data in terms of the minisuper-space model (75) was first reported in [36].

A discretized, dimensionless version of (75) is

$$S_{discr} = k_1 \sum_i \left(\frac{(N_3(i+1) - N_3(i))^2}{N_3(i)} + \tilde{k}_2 N_3^{1/3}(i) \right), \quad (76)$$

where $\tilde{k}_2 \propto k_2$. This can be seen by applying the scaling (71), namely, $N_3(i) = N_4^{3/4} n_3(s_i)$ and $s_i = i/N_4^{1/4}$. This enables us to finally conclude that the identifications (73) when used in the action (76) lead naïvely to the continuum expression (75) under the identification⁶

$$G = \frac{a^2 \sqrt{\tilde{C}_4} \tilde{s}_0^2}{k_1 3\sqrt{6}}. \quad (77)$$

We also note that the reported scaling (71) implies that we can write

$$S_{discr} = k_1 \sqrt{N_4} \sum_i ds_i \left(\frac{1}{n_3(s_i)} \left(\frac{n_3(s_{i+1}) - n_3(s_i)}{ds_i} \right)^2 + \tilde{k}_2 n_3^{1/3}(s_i) \right), \quad (78)$$

where $ds_i = 1/N_4^{1/4}$. Thus, referring to (65), we see that there are at least terms in $\log f(N_4, \kappa_0, \Delta)$ which scale like $\sqrt{N_4}$. To obtain the form (65) we need additional terms of entropic nature since the coefficient of $\sqrt{N_4}$ in (65) is assumed positive.

4.2 The size of the universe and the flow of G

It is natural to identify the coupling constant G multiplying the effective action for the scale factor with the gravitational coupling constant G . The effective action describing our computer-generated data is given by eq. (75), and its dimensionless lattice version by (76). The computer data allow us to extract $k_1 \propto a^2/G$, with a the spatial lattice spacing, and the precise constant of proportionality given by eq. (77).

For the bare coupling constants $(\kappa_0, \Delta) = (2.2, 0.6)$ we have high-statistics measurements for N_4 ranging between 45.500 and 362.000 four-simplices (equivalently, $N_4^{(4,1)}$ ranging between 20.000 and 160.000 four-simplices). The choice of Δ determines the asymmetry parameter α , and the choice of (κ_0, Δ) determines the ratio ξ between $N_4^{(3,2)}$ and $N_4^{(4,1)}$. This in turn determines the “effective” four-volume \tilde{C}_4 of an average four-simplex, which also appears in (77). The number \tilde{s}_0 in (77) is determined directly from the time extension T_{univ} of the extended universe according to

$$T_{univ} = \pi \tilde{s}_0 \left(N_4^{(4,1)} \right)^{1/4}. \quad (79)$$

Finally, from our measurements we have determined $k_1 = 0.038$. Taking everything together according to (77), we obtain $G \approx 0.23a^2$, or $\ell_{pl} \approx 0.48a$, where $\ell_{pl} = \sqrt{G}$ is the Planck length.

⁶ Due to the difference in four-volume between $N_4^{(3,2)}$ and $N_4^{(4,1)}$ for $\alpha \neq 1$ we have to introduce a compensating factor $\tilde{s}_0 \equiv s_0 \langle N_4 \rangle^{1/4} / \langle N_4^{(4,1)} \rangle^{1/4}$, see [21] for a detailed discussion.

From the identification of the volume of the four-sphere, $V_4 = 8\pi^2 R^4/3 = \tilde{C}_4 N_4^{(4,1)} a^4$, we obtain that $R = 3.1a$. In other words, *the linear size πR of the quantum de Sitter universes studied here lies in the range of 12-21 Planck lengths for N_4 in the range mentioned above and for the bare coupling constants chosen as $(\kappa_0, \Delta) = (2.2, 0.6)$.*

Our dynamically generated universes are therefore not very big, and the quantum fluctuations around their average shape are large, as is apparent from Fig. 8. The presence of such fluctuations is evident in the bottom snapshot picture of the extended universe shown in Fig. 7, whose volume profile deviates from that of a regular sphere. The point is of course that we have to perform an averaging process to obtain the *expectation value* of the volume profile, and this is precisely what we have been doing numerically. It is rather surprising that the semiclassical minisuper-space formulation gives an adequate description – at least for the volume profile – for universes of such a small size, a fact that should be welcome news to anyone performing semiclassical calculations to describe the behaviour of the early universe. However, when looking at more local geometric properties of the universe, our lattices are still coarse compared to the Planck scale ℓ_{Pl} because the latter corresponds to roughly half a lattice spacing. If we are after a theory of quantum gravity valid on all scales, we are specifically interested in uncovering phenomena associated with Planck-scale physics. In order to collect data which are free from unphysical short-distance lattice artefacts at this scale, we would ideally like to work with a lattice spacing much smaller than the Planck length, while still being able to set by hand the physical volume of the universe studied on the computer. The way to achieve this is by changing the bare coupling constants κ_0, Δ such that the coefficient K in (77), $G =: Ka^2$, is changed to a larger value. However, K is a combination of a number of factors and they might change differently when κ_0, Δ are changed. It is thus a (computer-)experimental exercise to find a path in the (κ_0, Δ) coupling-constant plane such that K increases and we end up with $\ell_{Pl} = \sqrt{K}a \gg a$. We will discuss later whether such a path exists.

5 Constructive evidence for the effective action

We have found a perfect fit (71) to the emergent background geometry and the curve can be related to the continuum effective action (75). However, it is still of interest to investigate to what extent the action (76) can be rederived from the data. Interestingly, as we shall see below, this can largely be done.

The data at our disposal are: (i) the measurement of the three-volume $N_3(i)$ at the discrete time step i , and of the three-volume correlator $N_3(i)N_3(j)$. Having created Q statistically independent configurations $N_3^{(q)}(i)$ by Monte Carlo simulation allows us to construct the average

$$\bar{N}_3(i) := \langle N_3(i) \rangle \cong \frac{1}{Q} \sum_{q=1}^Q N_3^{(q)}(i), \quad (80)$$

where the superscript in $(\cdot)^{(q)}$ denotes the result of the q 'th configuration sampled; (ii) the covariance matrix

$$C(i, j) \cong \frac{1}{Q} \sum_{q=1}^Q (N_3^{(q)}(i) - \bar{N}_3(i))(N_3^{(q)}(j) - \bar{N}_3(j)). \quad (81)$$

We now assume we have a discretized action which can be expanded around the expectation value $\bar{N}_3(i)$ according to

$$S_{discr}[\bar{N} + n] = S_{discr}[\bar{N}] + \frac{1}{2} \sum_{i,j} n_i \hat{P}_{ij} n_j + O(n^3). \quad (82)$$

If the quadratic approximation describes the quantum fluctuations around the expectation value \bar{N} well, the inverse of the operator \hat{P} will be a good approximation to the covariance matrix. Conversely, still assuming the quadratic approximation gives a good description of the fluctuations, the \hat{P} constructed from the covariance matrix will to a good approximation allow us to reconstruct the action via (82).

Fig. 10 shows the measured covariance matrix $C(i, j)$ and its inverse, the operator \hat{P} . Some care is needed in inverting $C(i, j)$ since it has two zero modes, one from the constraint that N_4 is kept fixed, and (an approximate) one from the fact that the translational mode of the ‘centre of volume’ can only be fixed up to a lattice spacing, see [21] for a detailed discussion. As is clear from the figure, the inverse \hat{P} is completely dominated by the stalk data. This feature is unavoidable: while the correlation matrix is dominated by long-range fluctuations, the inverse matrix will be dominated by short-distance fluctuations, i.e. the fluctuations in the stalk, which by definition are associated with cut-off energies.

Looking at the inverse \hat{P} of the measured covariance matrix, we observe that to very good approximation it is small and constant, except on the diagonal and the entries neighbouring the diagonal. This means that we can decompose it into a ‘kinetic’ and a ‘potential’ term. The kinetic part \hat{P}^{kin} is defined as the matrix with non-zero elements on the diagonal and in the neighbouring entries, such that the sum of the elements in a row or column is always zero. The potential part \hat{P}^{pot} is then given by whatever remains along the diagonal. We therefore arrive at a tentative representation of \hat{P} as

$$\hat{P}_{ij} = \hat{P}_{ij}^{kin} + \hat{P}_{ij}^{pot}, \quad (83)$$

$$\hat{P}_{ij}^{kin} = p_i \Delta_{ij}, \quad \hat{P}_{ij}^{pot} = u_i \delta_{ij}, \quad (84)$$

where the matrices Δ_{ij} and δ_{ij} are essentially defined through the construction just described⁷. We know \hat{P} from the data, and can make a least- χ^2 fit to determine the

⁷ For details of normalization and subtleties in the definition of \hat{P}^{kin} and \hat{P}^{pot} related to the zero modes we refer to [21].

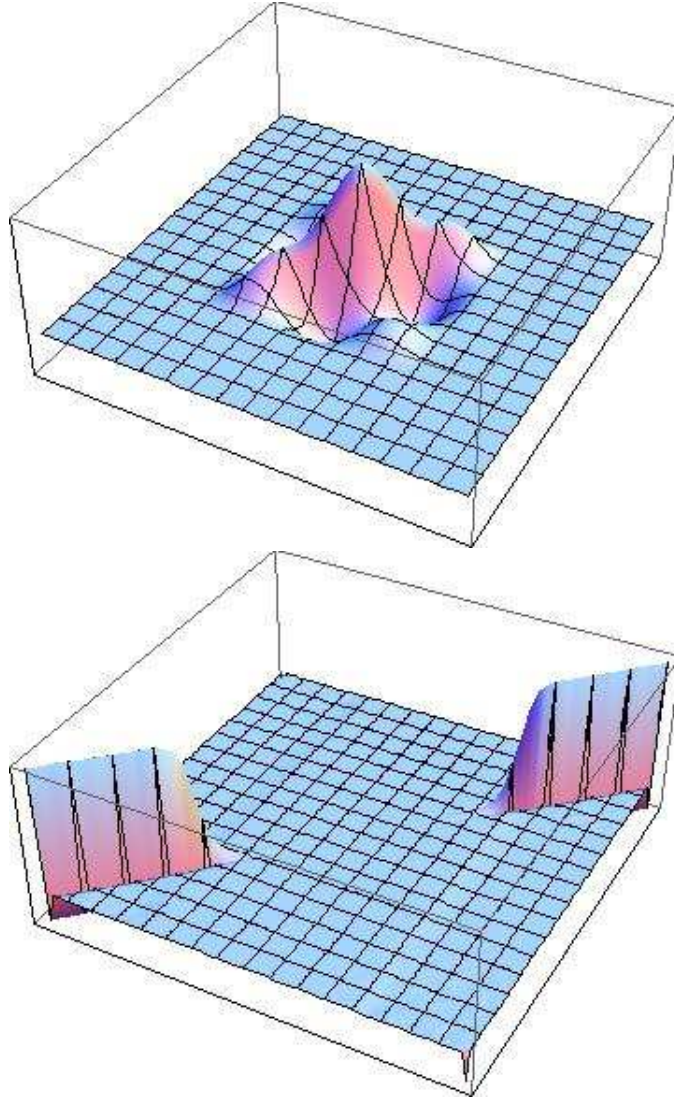


Fig. 10 The covariance matrix C (top) and its inverse (bottom).

numbers p_i and u_i . For details we refer again to [21]. The results are shown in Figs. 11 and 12.

Let us look at the discretized minisuperspace action (76) which has served as inspiration for the definition of \hat{P}^{kin} and \hat{P}^{pot} . Expanding $N_3(i)$ to second order around $\bar{N}_3(i)$, one obtains the identifications

$$\bar{N}_3(i) = \frac{2k_1}{p_i}, \quad U''(\bar{N}_3(i)) = -u_i, \quad (85)$$

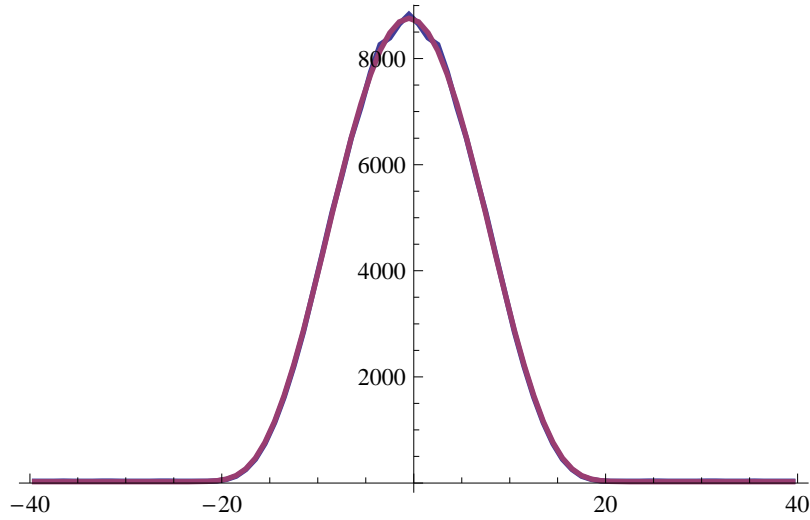


Fig. 11 The directly measured expectation values $\bar{N}_3(i)$ compared to the averages $\bar{N}_3(i)$ reconstructed from (85), for $\kappa_0 = 2.2$ and $\Delta = 0.6$.

where $U(N_3(i)) = k_1 \tilde{k}_2 N_3^{1/3}(i)$ denotes the potential term in (76). We use the fitted coefficients p_i to reconstruct $\bar{N}_3(i)$ and then compare these reconstructed values with the averages $\bar{N}_3(i)$ measured directly. Similarly, we can use the measured u_i 's to reconstruct the second derivatives $U''(\bar{N}_3(i))$ and compare them to the form $\bar{N}_3^{-5/3}(i)$ coming from (76).

The reconstruction of $\bar{N}_3(i)$ is illustrated in Fig. 11 for a given four-volume N_4 and compared with the directly measured expectation values $\bar{N}_3(i)$. One observes that the reconstruction works very well and, most importantly, that the coupling constant k_1 , which in this way can be determined independently for each four-volume N_4 , really *is* independent of N_4 's we have considered, as it should be.

We will now try to extract the potential $U''(\bar{N}_3(i))$ from the information contained in the matrix \hat{P}^{pot} . The determination of $U''(\bar{N}_3(i))$ is not an easy task as can be understood from Fig. 12, which shows the measured coefficients u_i extracted from the matrix \hat{P}^{pot} , and which we consider rather remarkable. The interpolated curve makes an abrupt jump by two orders of magnitude going from the extended part of the universe (stretching over roughly 40 time steps) to the stalk. The occurrence of this jump is entirely dynamical, since no distinction has ever been made by hand between stalk and bulk. In order to extract physical information related to a genuine potential like the one appearing in (76), we of course must restrict ourselves to the region inside the “blob”, corresponding to the data range encircled in Fig. 12. From the figure it is also clear that extracting $U''(\bar{N}_3(i))$ from the data available is a nontrivial task.

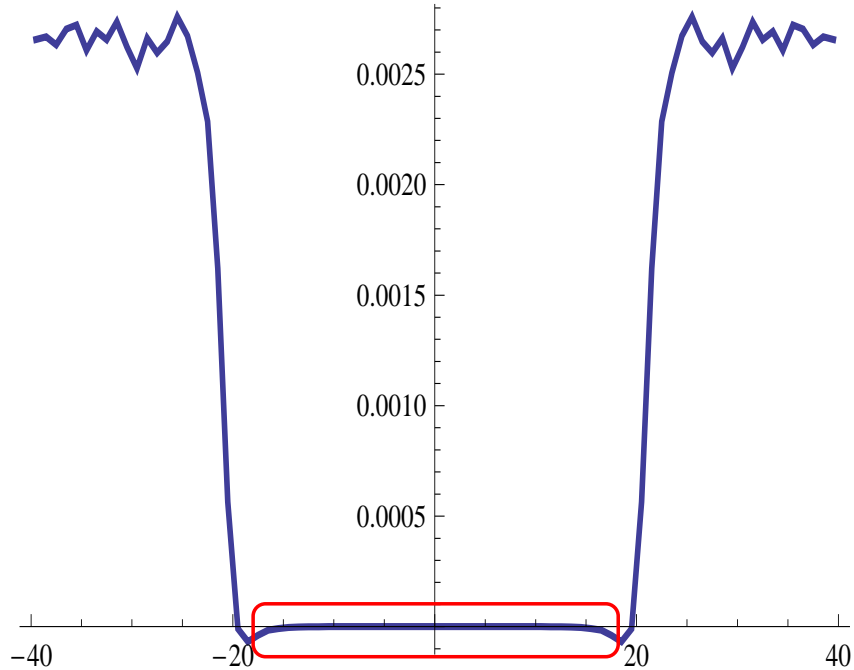


Fig. 12 Reconstructing the second derivative $U''(\bar{N}_3(i))$ from the coefficients u_i , for $\kappa_0 = 2.2$, $\Delta = 0.6$ and $N_4^{(4,1)} = 160.000$. Data chosen from the encircled region are independent of short-distance artefacts.

The range of the discrete three-volumes $N_3(i)$ in the extended universe is from several thousand down to five, the kinematically allowed minimum. However, the behaviour for the very small values of $N_3(i)$ near the edge of the extended universe is likely to be mixed in with discretization effects. In order to test whether one really has a $N_3^{1/3}(i)$ -term in the action one should therefore only use values of $N_3(i)$ somewhat larger than five (shown as the encircled region in Fig. 12). This has been done in Fig. 13, where we have converted the coefficients u_i from functions of the discrete time steps i into functions of the background spatial three-volume $\bar{N}_3(i)$ using the identification in (85) (the conversion factor can be read off the relevant curve in Fig. 11). The data presented in Fig. 13 were taken at a discrete volume $N_4^{(4,1)} = 160.000$, and fit well the form $N_3^{-5/3}$, corresponding to a potential $\tilde{k}_2 N_3^{1/3}$.

Apart from obtaining the correct power $N_3^{-5/3}$ for the potential for a given space-time volume N_4 , it is equally important that the coefficient in front of this term be independent of N_4 . This seems to be the case as is shown in Fig. 14, where we have plotted the measured potentials in terms of reduced, dimensionless variables which make the comparison between measurements for different N_4 's easier. – In summary, we conclude that the data allow us to reconstruct the action (76) with good precision.

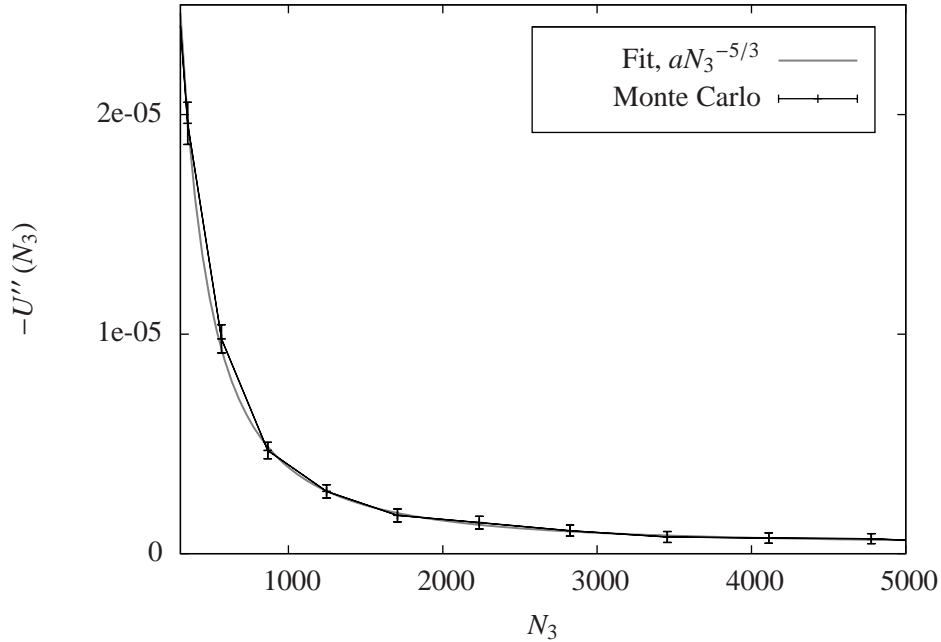


Fig. 13 The second derivative $-U''(N_3)$ as measured for $N_4^{(4,1)} = 160,000$, $\kappa_0 = 2.2$ and $\Delta = 0.6$.

6 Connection to Hořava-Lifshitz gravity

While we have verified that the action (76) describes the data well, one aspect of the formula may lend itself to a more general interpretation. Until now we have chosen to view the “experimental” formula (71) as describing a round four-sphere via the identifications (72) and (73). However, the potential asymmetry between space and time introduced in our model by working with a time foliation allows for a different interpretation, namely, that space and time really behave differently, as we will explain in what follows.

Although at the level of the piecewise linear structures we have a precise relation between the coupling constant Δ and the asymmetry parameter α , this relation enters the construction only in a relatively weak way, in that for a given Δ the bare action we use is the Regge-Einstein-Hilbert action for a piecewise linear manifold with the given connectivity and the length assignment $a_t^2 = \alpha a_s^2$. Nowhere else does this length assignment appear. Of course, *if* the model had a well-defined perturbative expansion, one could have chosen the bare coupling constants such that the classical action (and, by implication, the relation between a_s and a_t) played an important role in the path integral. However, as already explained in the introduction, this is not the case. Rather, our choice of bare coupling constants is dictated by the

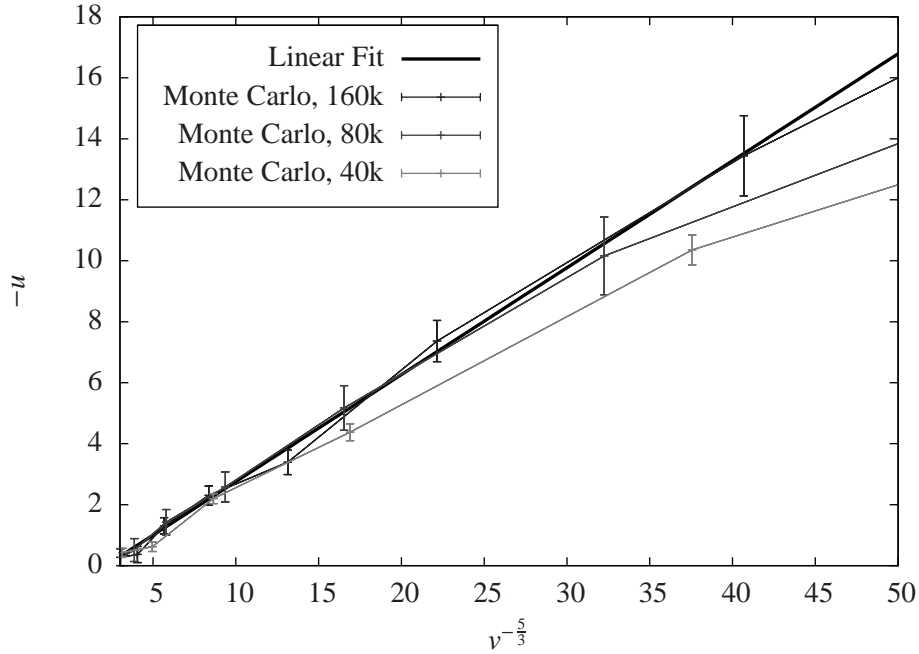


Fig. 14 The dimensionless second derivative $u = N_4^{5/4} U''(N_3)$ plotted against $v^{-5/3}$, where $v = N_3/N_4^{3/4}$ is the dimensionless spatial volume, for $N_4^{(4,1)} = 40.000, 80.000$ and 160.000 , $\kappa_0 = 2.2$ and $\Delta = 0.6$. One expects a universal straight line near the origin (i.e. for large volumes) if the power law $U(N_3) \propto N^{1/3}$ is correct.

wish to find nontrivial physics, which restricts us to a region far away from where the action term dominates the entropy of configurations.

In other words, the effective action we have obtained bears only indirect traces of the classical action put into the path integral. Similarly, the precise relation between space and time directions in the final continuum theory will be determined by the statistical averages resulting from the full path integral, rather than the parameter α put into the discretized action.

To illustrate the nonperturbative mechanism at work, let us consider the measurements in phase C, where we observe a macroscopic universe whose extension in the time direction scales like $N_4^{1/4}$ for different, fixed four-volumes N_4 . It should be emphasized that this scaling behaviour is by no means predetermined, for example, time in phase B scales completely differently (in fact, the time extension vanishes there, which is of course an extreme situation). One is therefore led to conclude that time and (the linear extension of) space scale identically in phase C. This is corroborated by evidence that well inside phase C there seems to be a well-defined notion of a “physical” proper time extent independent of α , as one would have expected naïvely [22].

However, the fact that the behaviour in phase B is very different leaves open the interesting possibility that a nontrivial scaling relation between time and spatial extent may ensue *when one approaches the B-C phase transition line*. In that case one could try to describe the situation by a continuum effective action where time and space have different dimensionality. This is precisely what P. Hořava attempted in his novel class of gravity theories [23], a topic we will return to shortly. But even in phase C, where time and space scale in the same way, one could explore the consequences of relaxing the notion that time and space should be related exactly as they are in general relativity. What we have done until now is to interpret our results in the continuum limit in terms of the classical theory. This can be achieved by making a global rescaling of continuum proper time, which we have direct access to through the preferred time foliation. More specifically, we have been checking our data against the cosmological minisuperspace model (75), which can be derived from general relativity by assuming spatial homogeneity and isotropy. Eq. (75), when written in terms of the scale factor⁸ $a(\tau)$, τ denoting proper time, reads

$$S = \frac{3\pi}{4} \int d\tau \left(aa'^2 + a - \lambda a^3 \right). \quad (86)$$

All our measurements are perfectly consistent with an effective action of this form, but the “cosmological” observables we have been considering so far cannot discriminate between this and more general cosmologies coming from a generalized “gravity” theory with a built-in anisotropy between space and time, like Hořava’s. In the latter, one can again assume *spatial* homogeneity and isotropy to obtain cosmological solutions, which in the Euclidean sector, *in the infrared limit*, arise from an action quite similar to (86) [24, 25, 26], namely,

$$S = \frac{\pi}{8} \int d\tau \left(3(3\hat{\lambda} - 1)aa'^2 + 6\gamma a - a^3(6\lambda + \tilde{V}(a)) \right). \quad (87)$$

The “potential” $\tilde{V}(a)$ in this expression has an expansion in inverse powers of a , coming from the higher-order spatial derivative terms in the Hořava-Lifshitz action. In the actual computer simulations, in both (86) and (87) λ is a Lagrange multiplier rather than a cosmological constant, which ensures that the four-volume is kept fixed. As long as we can fix proper time only up to a constant and as long as we cannot measure reliably the correction term $\tilde{V}(a)$ containing inverse powers of a , it is not really possible to distinguish “experimentally” between (86) and (87) in terms of a reconstruction of the action, as we did in the previous Section. In this situation, whenever $\hat{\lambda} > 1/3$ and $\gamma > 0$, a rescaling of time in (87) leads to the same form as (86) up to a constant of proportionality. Taking into account the difficulties in verifying the mere existence of the linear term in (86) from the data (cf. Fig. 12), it is clear that we cannot presently extract from the data in a reliable way a potential $\tilde{V}(a)$ that depends on inverse powers of a , starting with a^{-4} . The only region in Fig. 12 where such information could be extracted is for the smallest values of a .

⁸ equivalently, one can also work with the associated three-volume $V(\tau) = 2\pi^2 a(\tau)^3$ as the basic configuration space variable

Unfortunately, this is also where lattice artefacts will be important and artefacts from the “stalk” may get mixed in with genuine continuum physics; a glance at Fig. 12 reveals how large the effects of the stalk are right next to the small- a region.

This notwithstanding, we can discuss the qualitative correspondence between the Hořava scenario and our phase diagram. In our earlier analysis of the different phases of CDT quantum gravity, we have chosen for a particular qualitative description to match precisely that of a Lifshitz phase diagram [27, 28]. The qualitative feature we want to emphasize in this context is that the role played by “average geometry” in quantum gravity bears an intriguing resemblance to that played by the Lifshitz field ϕ . In an effective Lifshitz theory, the Landau free energy density $F(x)$ as function of an order parameter $\phi(x)$ takes the form⁹

$$F(x) = a_2\phi(x)^2 + a_4\phi(x)^4 + a_6\phi(x)^6 + \dots + c_2(\partial_\alpha\phi)^2 + d_2(\partial_\beta\phi)^2 + e_2(\partial_\beta^2\phi)^2 + \dots, \quad (88)$$

where for a d -dimensional system $\alpha = m + 1, \dots, d$, $\beta = 1, \dots, m$. Distinguishing between “ α ”- and “ β ”-directions allows one to take anisotropic behaviour into account. For a usual system, $m = 0$ and a phase transition can occur when a_2 passes through zero (say, as a function of temperature). For $a_2 > 0$ we have $\phi = 0$, while for $a_2 < 0$ we have $|\phi| > 0$ (always assuming $a_4 > 0$). However, one also has a transition when anisotropy is present ($m > 0$) and d_2 passes through zero. For negative d_2 one can then have an oscillating behaviour of ϕ in the m “ β ”-directions. Depending on the sign of a_2 , the transition to this so-called modulated or helical phase can occur either from the phase where $\phi = 0$, or from the phase where $|\phi| > 0$. We conclude that the phases C, B, and A of CDT quantum gravity depicted in Fig. 8 can be put into one-to-one correspondence with the ferromagnetic, paramagnetic and helical phases of the Lifshitz phase diagram¹⁰ if we in place of ϕ we use “average geometry”. The triple point where the three phases meet is the so-called Lifshitz point, where in the Lifshitz model one can have a nontrivial scaling.

The critical dimension beyond which the mean-field Lifshitz theory alluded to above is believed to be valid is $d_c = 4 + m/2$. In lower dimensions, the fluctuations play an important role and so does the number of components of the field ϕ . This does not necessarily affect the general structure of the phase diagram, but can alter the order of the transitions. Without entering into the details of the rather complex general situation, let us just mention that for $m = 1$ fluctuations will often turn the transition along the A-C phase boundary into a first-order transition. Likewise, most often the transition between phases B and C is of second order.

We conclude that the structure of the Lifshitz phase diagram is presently compatible with our CDT observations. Based on the order parameter investigated in [17], the A-C transition of CDT quantum gravity looks like a clear-cut first-order transition. On the other hand, the verdict is still out for the B-C line. The signals from the Monte Carlo simulations are ambiguous, and it appears that close to the

⁹ see, for example, [28] for an introduction to the content and scope of “Landau theory”

¹⁰ For definiteness, we are using here a “magnetic” language for the Lifshitz diagram. However, the Lifshitz diagram can also describe a variety of other systems, for instance, liquid crystals.

transition line our algorithms for updating the geometries need to be improved to produce fully reliable results.

Phase transitions of higher than first order are of intrinsic interest since they may serve as points where one can define the continuum theory. Since it appears that we have a well-defined infrared limit in phase C, such points would naturally be UV fixed points, and moving away from them should bring us to the IR limit. Given the overall structure of the phase diagram, the possible scenarios are as follows: if either the A-C or the B-C line is second-order, we can potentially use any point on it to attempt to define a UV limit. By contrast, if they are first-order lines, we are left with two interesting points which may be associated with a higher-order transition: the endpoint P_0 of the open B-C line (cf. Fig. 6), where the phase transition may be of higher order than along the line itself, and the Lifshitz triple point P_t , where the transition may also be of higher order.

Assuming there were such higher-order phase transition points, how would we determine whether the UV limit of the theory is isotropic in space and time or, more generally, of Hořava-type? One defining aspect of Hořava-Lifshitz gravity is the assumption that the scaling dimensions of space and time differ in the ultraviolet regime. This difference is used to construct a theory containing higher-order spatial derivatives in such a way that it is renormalizable. How would one observe such a difference in the present lattice approach? – Consider a universe of time extent T , spatial extension L and total four-volume $V_4(T, L)$. By measuring T and L we can establish the mutual relations

$$T \propto V_4^{1/d_t}, \quad L \propto \left(V_4^{1-1/d_t} \right)^{1/d_s} \propto T^{(d_t-1)/d_s}. \quad (89)$$

Well inside phase C we have measured $d_t = 4$ and $d_s = 3$, in agreement with what is expected for an ordinary four-dimensional spacetime. If the dimension [T] of time was z times the dimension [L] of length, we would have

$$z = \frac{d_s}{d_t - 1}. \quad (90)$$

We observed earlier that well inside phase B both d_s and d_t must be large, if not infinite. In case the B-C phase transition is second-order, it may happen that z goes to a value different from 1 when we approach the transition line. To investigate this possibility, we have tried to determine z as a function of the parameter Δ as $\Delta \rightarrow 0$. For $\Delta > 0.3$ one obtains convincingly $d_t \approx 4$ and $d_s \approx 3$ and thus $z \approx 1$. We can make an even stronger statement, namely, that the data does not contradict the interpretation of Δ as an (unphysical) asymmetry parameter: when Δ is increased the corresponding α is decreasing (see Fig. 4), while the number of lattice spacings in the time direction is increasing, which at least qualitatively allows for the interpretation that the physical “time” is independent of α . By contrast, for $\Delta \lesssim 0.3$ the quality of our results does not allow for any definite statements. Autocorrelation times become very long and there may be large finite-volume effects, which obscure the measurements and which are precisely based on finite-size scaling.

To summarize, there is still a distinct possibility that a nontrivial scaling with $z \neq 1$ can occur when one approaches the transition line between phases B and C. Should the B-C transition turn out to be a first-order transition, the interesting points would be P_0 and P_t . It would then be natural to conjecture that the point P_t is a Hořava-Lifshitz point with a nontrivial scaling relation between space and time. The point P_0 , which does not appear in a standard Lifshitz diagram, would perhaps be a natural candidate for an isotropic scaling point. On the other hand, if the B-C transition line is second-order, it leaves open the interesting possibility that the critical exponent changes continuously from $z = 3$ at the Lifshitz point P_t to $z = 1$ at the (hypothetically) isotropic point P_0 .

7 Making contact with asymptotic safety

As we discussed earlier, it is presently difficult to get close to the B-C phase transition line, which is needed if we want to achieve a higher resolution in the UV regime, such that the lattice spacing is much smaller than the Planck length. Also, we do not know yet whether in such a limit we have isotropy in space and time, like in the asymptotic safety approach, or need to invoke an anisotropic scenario as outlined above. For the time being, let us assume that the endpoint P_0 of the B-C transition line in the phase diagram of Fig. 6 corresponds to an isotropic phase transition point. How can one make contact with the gravitational renormalization group treatment? The standard way would be to “measure” observables (by lattice Monte Carlo simulations), like a mass in QCD or the string tension in Yang-Mills theory. For definiteness, consider the string tension, which has mass dimension two. The measurements, for some choice g_0 of the bare coupling constant, will give us a number $\sigma(g_0)$. We now write

$$\sigma(g_0) = \sigma_R a^2(g_0), \quad (91)$$

where σ_R is the physical string tension and $a(g_0)$ describes the dependence of the lattice spacing a on the bare coupling constant. Being able to write down a relation like this for all observables, where $a(g_0)$ is determined by the renormalization group equation

$$a \frac{dg_0}{da} = -\beta(g_0), \quad (92)$$

allows us to define a continuum theory at a fixed point g_0^* where $\beta(g_0) = 0$, since there we can take $a(g_0) \rightarrow 0$ when $g_0 \rightarrow g_0^*$. In the case of QCD or Yang-Mills theory the fixed point is the Gaussian fixed point $g_0^* = 0$, but in the more general setting of asymptotic safety it will be non-Gaussian.

Assume now that we have a fixed point for gravity. The gravitational coupling constant is dimensionful, and we can write for the bare coupling constant

$$G(a) = a^2 \hat{G}(a), \quad a \frac{d\hat{G}}{da} = -\beta(\hat{G}), \quad \beta(\hat{G}) = 2\hat{G} - c\hat{G}^3 + \dots. \quad (93)$$

The IR fixed point $\hat{G} = 0$ corresponds to G constant while the putative non-Gaussian fixed point corresponds to $\hat{G} \rightarrow \hat{G}^*$, i.e. $G(a) \rightarrow \hat{G}^* a^2$. In our case it is tempting to identify our dimensionless constant k_1 with $1/\hat{G}$, up to the constant of proportionality given in (77). Close to the UV fixed point we have

$$\hat{G}(a) = \hat{G}^* - K a^{\tilde{c}}, \quad k_1 = k_1^* + K a^{\tilde{c}}, \quad \tilde{c} = -\beta'(\hat{G}^*). \quad (94)$$

Usually one relates the lattice spacing near the fixed point to the bare coupling constants with the help of some correlation length ξ . Assume that ξ diverges according to

$$\xi(g_0) = \frac{c}{|g_0 - g_0^*|^{\nu}} \quad (95)$$

in the limit as we tune the bare coupling constant $g_0 \rightarrow g_0^*$. This correlation length is associated with a field correlator and usually some physical mass m_{ph} by means of

$$\frac{|n_1 - n_2|}{\xi(g_0)} = m_{ph}(a|n_1 - n_2|) = m_{ph}|x_1 - x_2|, \quad (96)$$

where $|n_1 - n_2|$ is a discrete lattice distance and $|x_1 - x_2|$ a physical distance. Requiring the physical quantities $|x_1 - x_2|$ and m_{ph} to remain constant as $a \rightarrow 0$ then fixes a as a function of the bare coupling constant,

$$a = \frac{1}{c m_{ph}} |g_0 - g_0^*|^{\nu}. \quad (97)$$

Eq. (97) is only valid close to the fixed point and should be compared to the renormalization group equation (92), from which we deduce that $\nu = -1/|\beta'(g_0^*)|$.

In the gravitational case at hand we do not (yet) have observables which would allow us to define meaningful correlation lengths. At any rate, it is by no means a settled issue how to *define* such a concept in a theory where one integrates over all geometries, and where the length is itself a function of geometry (see [32] for related discussions). Instead, we construct from our computer-generated “data” an effective action, where all degrees of freedom, apart from the scale factor, have been integrated out. We impose the constraint that the data are fitted to a universe of total lattice four-volume N_4 . Measurements are performed at different, fixed values of N_4 , all the while maintaining the relation¹¹

$$V_4 = N_4 a^4. \quad (98)$$

We then “remove the regulator”, by investigating the limit $N_4 \rightarrow \infty$. In ordinary lattice field theory, we have two options for changing N_4 ; either we keep a fixed, and therefore change V_4 , or we keep V_4 fixed and change a . Let us illustrate the difference in terms of a scalar field on a lattice. Its dimensionless action can be written as

¹¹ in principle, we should be taking into account the different volumes of the two types of four-simplices, which depend on Δ , but we will ignore these details to streamline the presentation

$$S = \sum_i \left(\sum_{\mu} (\phi(i+\mu) - \phi(i))^2 + m_0^2 \phi^2(i) \right), \quad (99)$$

where i labels discrete lattice points and μ unit vectors in the different lattice directions. The correlation length is approximately $1/m_0$ lattice spacings. Holding a fixed and increasing N_4 is not going to change the correlation length in any significant way if N_4 is sufficiently large. Thus the interpretation for fixed a is straightforward: the physical volume V_4 is simply increased and finite-size effects will become smaller and smaller. However, we can also insist on an interpretation where V_4 is kept fixed, N_4 is increased and a decreased accordingly. In this case, the lattice becomes finer and finer with increasing N_4 . But now the physical interpretation of (99) will change with increasing N_4 , even if no bare coupling constant is changed, and the correlation length is still approximately $1/m_0$ lattice spacings. Since the *physical* lattice length a decreases proportional to $1/N_4^{1/4}$ the *physical* correlation length is going to zero, and the physical mass to infinity. This can be made explicit in (99) by introducing the lattice spacing a ,

$$S = \frac{1}{a^2} \sum_i a^4 \left(\sum_{\mu} \left(\frac{(\phi(i+\mu) - \phi(i))^2}{a^2} \right) + \frac{m_0^2}{a^2} \phi^2(i) \right). \quad (100)$$

The physical mass is $m_{ph} = m_0/a$ and goes to infinity unless we adjust m_0 . The factor $1/a^2$ in front of the sum can be reabsorbed in a redefinition of ϕ if desired.

In our case it is natural to consider V_4 as fixed if we want to make contact with the continuum framework of asymptotic safety, since this will allow us to vary a . Suppose we have identified a fixed point which we consider interesting, e.g. the point P_0 in our phase diagram. We now approach this point and measure k_1 . If it is a UV fixed point, eq. (94) tells us what to expect. Using (98), we can now convert this into an equation involving N_4 , and suitable for application in CDT simulations,

$$k_1(N_4) = k_1^c - \tilde{K} N_4^{-\tilde{c}/4}. \quad (101)$$

When we measured $k_1(N_4)$ deep inside phase C (at the point $(\kappa_2, \Delta) = (2.2, 0.6)$), we did not find any N_4 -dependence of k_1 . However, according to the insights just presented, we should observe such a dependence at or close to a UV fixed point. As already noted earlier, an explicit verification of such a relation will have to await more reliable computer simulations close to the phase transition lines.

In fact, we have already seen indications in CDT quantum gravity of a short-distance behaviour like that occurring in the asymptotic safety scenario. Recall the “naïve” renormalization conditions (64) and (68). They were introduced mainly to illustrate how a renormalization procedure could lead to finite renormalized cosmological and gravitational constants, both with a semiclassical interpretation. If we are close to the UV fixed point, we know that G will not be constant when we change scale, but \hat{G} will. Writing $G(a) = a^2 \hat{G}^*$, eqs. (64) and (68) are changed to

$$\kappa_4 - \kappa_4^c = \frac{\Lambda}{\hat{G}^*} a^2, \quad k_1(\kappa_0^c) = \frac{1}{\hat{G}^*}. \quad (102)$$

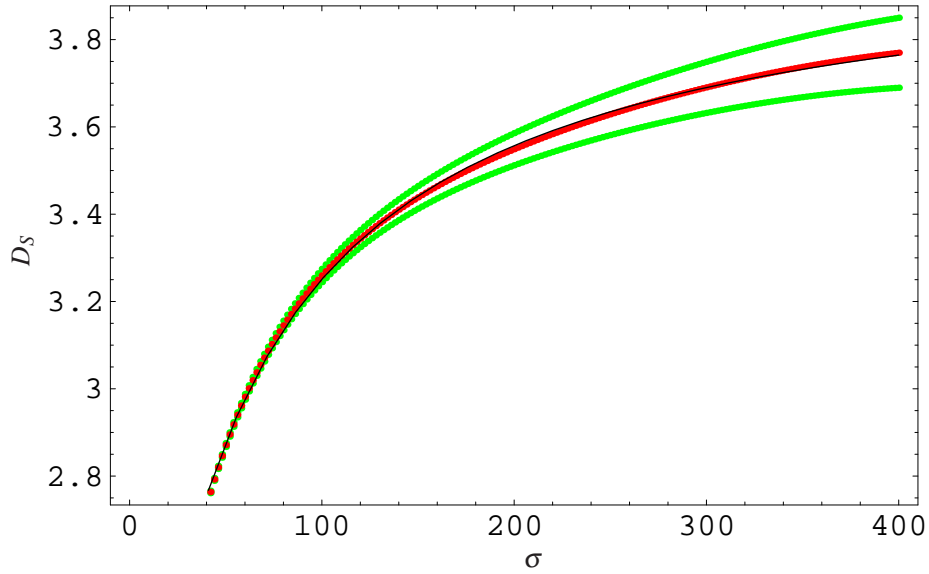


Fig. 15 The data points along the central curve show the spectral dimension $D_S(\sigma)$ of the universe as function of the diffusion time σ . Superimposed is a best fit, the continuous curve $D_S(\sigma) = 4.02 - 119/(54 + \sigma)$. The two outer curves quantify the error bars, which increase linearly with σ . (Measurements taken for a quantum universe with 181.000 four-simplices.)

The first of these relations now looks two-dimensional (cf. eq. (48))! Nevertheless, the expectation value of the four-volume still satisfies the correct relation

$$\langle V_4 \rangle = \langle N_4 \rangle a^4 \propto \frac{1}{\Lambda^2}, \quad (103)$$

as follows from (69).

Further hints of a two-dimensional signature at short distances have come from measuring the so-called spectral dimension. Essentially, this is the dimension a diffusing “liquid” would experience in a spacetime with a typical quantum geometry of the kind appearing in the gravitational path integral, see the original article [29] for details. Fig. 15 recalls the result of measuring the spectral dimension, which appears to change nontrivially as a function of diffusion time. Since short diffusion times probe short distances, we can read off from the fit indicated that the short-distance spectral dimension is close to two. What is most intriguing is that the short-distance result $D_S = 2$ has since been found in two other quantum field-theoretic approaches, namely, the renormalization group treatment à la Reuter [30] and Hořava-Lifshitz gravity [31]. At the same time, it means that this particular observable cannot distinguish between isotropic and anisotropic quantum gravity theories.

8 Discussion

The CDT model of quantum gravity, which we have described in these lectures is extraordinarily simple. It implements the path integral over causal geometries with a global time foliation. In order to perform the integration explicitly, we introduced a grid of piecewise linear geometries, similar to how one proceeds when defining the path integral in ordinary quantum mechanics. Next, we rotated each of these geometries to Euclidean signature and used as our bare action the Einstein-Hilbert action in Regge form. In terms of ingredients, that's all.

The resulting superposition exhibits a nontrivial scaling behaviour as function of the four-volume, and we observe the appearance of a well-defined average geometry, that of de Sitter space, the maximally symmetric solution to the classical Einstein equations in the presence of a positive cosmological constant. The measurements performed so far definitely probe the quantum regime, since the fluctuations of the three-volume around de Sitter space are sizable, as can be seen in Fig. 8. Both the average volume profile and the quantum fluctuations around it are well described in terms of the minisuperspace action (75). A key feature to appreciate here is that, unlike in standard (quantum-)cosmological treatments, this description is the *outcome* of a nonperturbative evaluation of the *full* path integral, with everything but the scale factor (equivalently, $V_3(t)$) summed over. Measuring the correlations of the quantum fluctuations in the computer simulations for a particular choice of bare coupling constants enabled us to determine the continuum gravitational coupling constant G as $G \approx 0.42a^2$, thereby introducing an absolute physical length scale into the dimensionless lattice setting. Within measuring accuracy, our de Sitter universes (with volumes lying in the range of 6.000-47.000 ℓ_{Pl}^4) are seen to behave perfectly semiclassically with regard to their large-scale properties.

These semiclassical results “emerge” even if, as emphasized above, we are far from a region in coupling-constant space where the classical action can be considered as dominant in the path integral. The resulting quantum geometry comes about through the interplay of the weight provided by the exponential of the bare action and the weight provided by the entropy of a particular kind of configuration. From this point of view the results are truly nonperturbative, even if they bear some similarity to the semiclassical minisuperspace results. It should also be emphasized that we have only derived an effective action for the scale factor, not for the “real”, transverse degrees of freedom. The issue of how to do this for the latter remains to be addressed.

The results we have reported are mostly “infrared” in nature. Our dynamically generated universes are macroscopic (although small) and – with the exception of the spectral dimension measurements – we are not yet probing Planckian (and possibly sub-Planckian) scales. It is a major issue whether such a short-distance completion of gravity exists in a conventional, field-theoretical sense. “Asymptotic safety” is an attempt to formulate the general conditions for this to be the case. In its simplest realization on the lattice it requires a UV fixed point. This is precisely the kind of situation the CDT framework allows us to address; we have a phase diagram and potential fixed points, and as outlined above it is in principle possible to check

whether the UV behaviour is in accordance with the predictions from asymptotic safety. Critical slowing down close to the potential fixed points, i.e. a vast increase in the computer time needed to generate statistically independent geometries, has so far made it impossible to obtain reliable results, but work is now in progress to improve the updating algorithms.

Once we succeed in approaching the phase transition line B-C in a reliable fashion, we may also be able to check whether the Hořava-Lifshitz scenario is realized in our model. In addition to the standard asymptotic safety picture, the CDT construction has the potential to accommodate also this scenario. Its obvious similarities with the defining properties of Hořava’s “anisotropic gravity” approach are the distinguished role of a time foliation, and the presence of a unitary time evolution (in CDT linked to the reflection positivity of the transfer matrix).

In addition to this, we have already pointed to the striking similarity between the CDT and Lifshitz phase diagrams upon (somewhat loosely) identifying the Lifshitz mean-field order parameter ϕ with “average geometry”. If more specifically we want to relate the Lifshitz field to a mode of the gravitational field, the conformal factor appears as a natural candidate. The conformal mode is already known to play a decisive role in a variety of geometro-dynamical contexts. In the bare Euclidean Einstein-Hilbert action the kinetic term associated with the conformal factor appears with the wrong, negative sign, leading to ill-defined expressions for naïve cosmological, Euclidean path integrals. In Euclidean noncritical string theory the dynamics of the conformal factor is believed to cause a transition from a “healthy phase” (where $c \leq 1$ for the central charge of matter) to a degenerate phase of so-called branched polymers (for $c > 1$)¹². A similar phenomenon was observed in the old Euclidean dynamical triangulations approach to quantum gravity, where the bare (inverse) gravitational coupling κ_0 plays the role of the central charge c , in the sense that for large values of κ_0 the configurations degenerate into branched polymers [39].

We have interpreted phase A (realized for large values of κ_0) as the CDT remnant of the branched-polymer phase, likewise caused by the dominance of the conformal mode. This suggests that the A-C phase transition may be interpreted as a transition where the kinetic term of the conformal mode changes sign. This is precisely what happens at the A-C transition in a Lifshitz diagram, corresponding to the expression (88) for the free energy of the order parameter ϕ .

The effective action for the conformal mode coming out of a nonperturbative gravitational path integral receives potential contributions from several sources: (i) from the bare action (where the kinetic conformal term has the “wrong”, negative sign), (ii) from the measure, and (iii) from integrating out other field components and, where applicable, other matter fields. It has been argued previously that the Faddeev-Popov determinants obtained from gauge-fixing the gravitational path integral contribute effectively with the opposite, positive sign to the conformal kinetic term [40, 41]. For example, when working in proper-time gauge, to imitate the time-

¹² In noncritical string theory there exists an analytic proof that for the dimension of (Euclidean) target spacetime $d \geq 2$ the string surfaces degenerate into branched polymers [34], see also [35] for similar results on a hypercubic lattice.

licing of CDT, Euclidean metrics can be decomposed according to¹³

$$ds^2 = d\tau^2 + e^{2\phi(\tau,x)} g_{ij}(\tau,x) dx^i dx^j, \quad (104)$$

giving rise to a term $-1/G^{(b)} e^{3\phi} \sqrt{\det g} (\partial_\tau \phi)^2$ in the bare gravity Lagrangian density, where $G^{(b)}$ is the bare Newton's constant. According to [41], one expects that the leading contribution from the associated Faddeev-Popov determinant has the same functional form, but with a plus instead of a minus sign, and with a different dependence on $G^{(b)}$. The presence of contributions of opposite sign to the effective action for the conformal mode $\phi(\tau, x)$ can therefore lead to two different behaviours, depending on the value of $G^{(b)}$ (equivalently, the κ_0 in our model), and thus account for the observed behaviour at the transition between phases A and C.¹⁴

In addition to the issues raised above, there is one more question which we would like to understand in more detail at this stage, which concerns the relation of our effective gravitational coupling constant G to a more conventional gravitational coupling constant, defined directly in terms of coupling gravity to matter. It would be desirable to verify that defining the physical Newton's constant G as the coupling constant multiplying the effective action for the three-volume, as we have been doing so far, agrees with a gravitational constant defined more directly through matter coupling. In principle it is easy to couple matter to CDT quantum gravity, as we already know from multiple studies in the Euclidean case [43], where spin, scalar and gauge fields have been considered. It is less straightforward to come up with a reasonably simple set-up for extracting the semiclassical effect of gravity on the matter sector (or vice versa), which is both well-defined on the ensemble of geometries and allows for effective computer measurements. Attempts in this direction were already undertaken in the "old" Euclidean approach [44, 45], and it is possible that similar ideas can also be used in our causal version of the theory. As a first step in this direction, the expected effect of a single point mass coupled to CDT quantum gravity on the volume profile of the universe has been quantified in [46]. Further work on coupled systems of matter and geometry is in progress.

Acknowledgments

JJ acknowledges partial support by the Polish Ministry of Science grant 182/N-QGG/2008/0 "Quantum Geometry and Quantum Gravity". AG has been supported by the Polish Ministry of Science grant N N202 034236 (2009-2010) and N N202 229137 (2009-2012). RL acknowledges support by the Netherlands Organisation for Scientific Research (NWO) under their VICI program.

¹³ The conformal decomposition of the spatial three-metric is essentially unique if one requires g_{ij} to have constant scalar curvature.

¹⁴ Related mechanisms have earlier been considered in the context of purely Euclidean dynamical triangulations by J. Smit [42].

References

1. S. Weinberg: *Ultraviolet divergences in quantum theories of gravitation*, in *General relativity: Einstein centenary survey*, eds. S.W. Hawking and W. Israel, Cambridge University Press, Cambridge, UK (1979) 790-831.
2. A. Codello, R. Percacci and C. Rahmede: *Investigating the ultraviolet properties of gravity with a Wilsonian renormalization group equation*, *Annals Phys.* **324** (2009) 414 [arXiv:0805.2909, hep-th];
M. Reuter and F. Saueressig: *Functional renormalization group equations, asymptotic safety, and Quantum Einstein Gravity* [arXiv:0708.1317, hep-th];
M. Niedermaier and M. Reuter: *The asymptotic safety scenario in quantum gravity*, *Living Rev. Rel.* **9** (2006) 5;
H.W. Hamber and R.M. Williams: *Nonlocal effective gravitational field equations and the running of Newton's G*, *Phys. Rev. D* **72** (2005) 044026 [hep-th/0507017];
D.F. Litim: *Fixed points of quantum gravity*, *Phys. Rev. Lett.* **92** (2004) 201301 [hep-th/0312114];
H. Kawai, Y. Kitazawa and M. Ninomiya: *Renormalizability of quantum gravity near two dimensions*, *Nucl. Phys. B* **467** (1996) 313-331 [hep-th/9511217].
3. A. Ashtekar, D. Marolf, J. Mourao and T. Thiemann: *Constructing Hamiltonian quantum theories from path integrals in a diffeomorphism-invariant context*, *Class. Quant. Grav.* **17** (2000) 4919-4940 [quant-ph/9904094].
4. C. Teitelboim: *Causality versus gauge invariance in quantum gravity and supergravity*, *Phys. Rev. Lett.* **50** (1983) 705-708;
The proper time gauge in quantum theory of gravitation, *Phys. Rev. D* **28** (1983) 297-309.
5. J. Louko and R.D. Sorkin, *Complex actions in two-dimensional topology change*, *Class. Quant. Grav.* **14** (1997) 179 [gr-qc/9511023].
6. J. Ambjørn, B. Durhuus and T. Jonsson: *Quantum geometry. A statistical field theory approach*, Cambridge, UK: Univ. Pr., 1997 (Cambridge Monographs in Mathematical Physics) 363 pp
7. J. Ambjørn and R. Loll: *Non-perturbative Lorentzian quantum gravity, causality and topology change*, *Nucl. Phys. B* **536** (1998) 407-434 [hep-th/9805108].
8. P. Di Francesco, E. Guitter and C. Kristjansen: *Generalized Lorentzian gravity in (1+1)D and the Calogero Hamiltonian*, *Nucl. Phys. B* **608** (2001) 485-526 [hep-th/0010259].
9. B. Durhuus and C.W. H. Lee: *A string bit Hamiltonian approach to two-dimensional quantum gravity*, *Nucl. Phys. B* **623** (2002) 201 [hep-th/0108149].
10. J. Ambjørn, K.N. Anagnostopoulos and R. Loll: *A new perspective on matter coupling in 2d quantum gravity*, *Phys. Rev. D* **60** (1999) 104035 [hep-th/9904012];
J. Ambjørn, K.N. Anagnostopoulos, R. Loll and I. Pushkina: *Shaken, but not stirred - Potts model coupled to quantum gravity*, *Nucl. Phys. B* **807** (2009) 251 [arXiv:0806.3506, hep-lat].
11. J. Ambjørn, R. Loll, W. Westra and S. Zohren: *Putting a cap on causality violations in CDT*, *JHEP* **0712** (2007) 017 [arXiv:0709.2784, gr-qc];
J. Ambjørn, R. Loll, Y. Watabiki, W. Westra and S. Zohren: *A string field theory based on causal dynamical triangulations*, *JHEP* **0805** (2008) 032 [arXiv:0802.0719, hep-th];
A matrix model for 2D quantum gravity defined by causal dynamical triangulations, *Phys. Lett. B* **665** (2008) 252-256 [arXiv:0804.0252, hep-th];
A new continuum limit of matrix models, *Phys. Lett. B* **670** (2008) 224 [arXiv:0810.2408, hep-th].
12. J. Ambjørn, R. Janik, W. Westra and S. Zohren: *The emergence of background geometry from quantum fluctuations*, *Phys. Lett. B* **641** (2006) 94 [gr-qc/0607013].
13. J. Ambjørn, J. Jurkiewicz and R. Loll: *Non-perturbative 3d Lorentzian quantum gravity*, *Phys. Rev. D* **64** (2001) 044011 [hep-th/0011276];
J. Ambjørn, J. Jurkiewicz, R. Loll and G. Vernizzi: *Lorentzian 3d gravity with wormholes via matrix models*, *JHEP* **0109** (2001) 022 [hep-th/0106082];
3D Lorentzian quantum gravity from the asymmetric ABAB matrix model, *Acta Phys. Polon.*

- B 34** (2003) 4667-4688 [hep-th/0311072];
 J. Ambjørn, J. Jurkiewicz and R. Loll: *Renormalization of 3d quantum gravity from matrix models*, Phys. Lett. B **581** (2004) 255-262 [hep-th/0307263];
 D. Benedetti, R. Loll and F. Zamponi: *(2+1)-dimensional quantum gravity as the continuum limit of causal dynamical triangulations*, Phys. Rev. D **76** (2007) 104022 [arXiv:0704.3214, hep-th].
14. J. Ambjørn, J. Jurkiewicz and R. Loll: *A non-perturbative Lorentzian path integral for gravity*, Phys. Rev. Lett. **85** (2000) 924 [hep-th/0002050];
Dynamically triangulating Lorentzian quantum gravity, Nucl. Phys. B **610** (2001) 347-382 [hep-th/0105267].
 15. T. Regge: *General relativity without coordinates*, Nuovo Cim. **19** (1961) 558.
 16. J. Ambjørn and J. Jurkiewicz: *On the exponential bound in four-dimensional simplicial gravity*, Phys. Lett. B **335** (1994) 355 [hep-lat/9405010].
 17. J. Ambjørn, A. Görlich, S. Jordan, J. Jurkiewicz and R. Loll: *CDT meets Horava-Lifshitz gravity*, Phys. Lett. B **690** (2010) 413-419 [arXiv:1002.3298, hep-th].
 18. J. Ambjørn, J. Jurkiewicz and R. Loll: *Emergence of a 4D world from causal quantum gravity*, Phys. Rev. Lett. **93** (2004) 131301 [hep-th/0404156].
 19. J. Ambjørn, J. Jurkiewicz and R. Loll: *Reconstructing the universe*, Phys. Rev. D **72** (2005) 064014 [hep-th/0505154].
 20. J. Ambjørn, A. Görlich, J. Jurkiewicz and R. Loll: *Planckian birth of the quantum de Sitter universe*, Phys. Rev. Lett. **100** (2008) 091304 [arXiv:0712.2485, hep-th].
 21. J. Ambjørn, A. Görlich, J. Jurkiewicz and R. Loll: *The nonperturbative quantum de Sitter universe*, Phys. Rev. D **78** (2008) 063544 [arXiv:0807.4481, hep-th].
 22. J. Ambjørn, A. Görlich, J. Jurkiewicz and R. Loll: *Geometry of the quantum universe*, Phys. Lett. B **690** (2010) 420-426 [arXiv:1001.4581, hep-th].
 23. P. Hořava: *Quantum gravity at a Lifshitz point*, Phys. Rev. D **79** (2009) 084008 [arXiv:0901.3775, hep-th].
 24. E. Kiritsis and G. Kofinas: *Hořava-Lifshitz cosmology*, Nucl. Phys. B **821** (2009) 467 [arXiv:0904.1334, hep-th].
 25. R. Brandenberger: *Matter bounce in Hořava-Lifshitz cosmology*, Phys. Rev. D **80** (2009) 043516 [arXiv:0904.2835, hep-th].
 26. G. Calcagni: *Cosmology of the Lifshitz universe*, JHEP **0909** (2009) 112 [arXiv:0904.0829, hep-th].
 27. R.M. Hornreich, M. Luban and S. Shtrikman: *Critical behavior at the onset of \mathbf{k} -space instability on the λ line*, Phys. Rev. Lett. **35** (1975) 1678.
 28. N. Goldenfeld: *Lectures on phase transitions and the renormalization group*, Addison-Wesley, Reading (Mass.) (1992).
 29. J. Ambjørn, J. Jurkiewicz and R. Loll: *Spectral dimension of the universe*, Phys. Rev. Lett. **95** (2005) 171301 [hep-th/0505113].
 30. O. Lauscher and M. Reuter: *Fractal spacetime structure in asymptotically safe gravity*, JHEP **0510** (2005) 050 [hep-th/0508202].
 31. P. Hořava: *Spectral dimension of the universe in quantum gravity at a Lifshitz point*, Phys. Rev. Lett. **102** (2009) 161301 [arXiv:0902.3657, hep-th].
 32. J. Ambjørn, J. Jurkiewicz and Y. Watabiki: *On the fractal structure of two-dimensional quantum gravity*, Nucl. Phys. B **454** (1995) 313 [hep-lat/9507014];
 J. Ambjørn and Y. Watabiki: *Scaling in quantum gravity*, Nucl. Phys. B **445** (1995) 129 [hep-th/9501049];
 J. Ambjørn and K.N. Anagnostopoulos: *Quantum geometry of 2D gravity coupled to unitary matter*, Nucl. Phys. B **497** (1997) 445 [hep-lat/9701006];
 J. Ambjørn, K.N. Anagnostopoulos, U. Magnea and G. Thorleifsson: *Geometrical interpretation of the KPZ exponents*, Phys. Lett. B **388** (1996) 713 [hep-lat/9606012].
 33. R. Nakayama: *2-D quantum gravity in the proper time gauge*, Phys. Lett. B **325** (1994) 347 [hep-th/9312158].
 34. J. Ambjørn and B. Durhuus: *Regularized bosonic strings need extrinsic curvature*, Phys. Lett. B **188** (1987) 253.

35. B. Durhuus, J. Fröhlich and T. Jonsson: *Critical behavior in a model of planar random surfaces*, Nucl. Phys. B **240** (1984) 453, Phys. Lett. **137B** (1984) 93.
36. J. Ambjørn, J. Jurkiewicz and R. Loll: *Semiclassical universe from first principles*, Phys. Lett. B **607** (2005) 205-213 [hep-th/0411152].
37. J. Ambjørn, J. Jurkiewicz and R. Loll: *The self-organized de Sitter universe*, Int. J. Mod. Phys. D **17** (2009) 2515 [arXiv:0806.0397, gr-qc].
38. J. Ambjørn, J. Jurkiewicz and R. Loll: *The universe from scratch*, Contemp. Phys. **47** (2006) 103-117 [hep-th/0509010];
R. Loll: *The emergence of spacetime, or, quantum gravity on your desktop*, Class. Quant. Grav. **25** (2008) 114006 [arXiv:0711.0273, gr-qc].
39. J. Ambjørn and J. Jurkiewicz: *Four-dimensional simplicial quantum gravity*, Phys. Lett. B **278** (1992) 42;
Scaling in four-dimensional quantum gravity, Nucl. Phys. B **451** (1995) 643 [hep-th/9503006].
40. P.O. Mazur and E. Mottola: *The path integral measure, conformal factor problem and stability of the ground state of quantum gravity*, Nucl. Phys. B **341** (1990) 187-212.
41. A. Dasgupta and R. Loll: *A proper-time cure for the conformal sickness in quantum gravity*, Nucl. Phys. B **606** (2001) 357-379 [hep-th/0103186].
42. J. Smit: *Remarks on the quantum gravity interpretation of 4D dynamical triangulation*, Nucl. Phys. Proc. Suppl. **53** (1997) 786 [hep-lat/9608082].
43. J. Ambjørn, Z. Burda, J. Jurkiewicz and C.F. Kristjansen: *4-d quantum gravity coupled to matter*, Phys. Rev. D **48** (1993) 3695-3703 [hep-th/9303042];
J. Ambjørn, J. Jurkiewicz, S. Bilke, Z. Burda and B. Petersson: *Z(2) gauge matter coupled to 4-D simplicial quantum gravity*, Mod. Phys. Lett. A **9** (1994) 2527-2542;
J. Ambjørn, K.N. Anagnostopoulos and J. Jurkiewicz: *Abelian gauge fields coupled to simplicial quantum gravity*, JHEP **9908** (1999) 016 [hep-lat/9907027].
44. B.V. de Bakker and J. Smit: *Gravitational binding in 4D dynamical triangulation*, Nucl. Phys. B **484** (1997) 476-494 [hep-lat/9604023].
45. H.W. Hamber and R.M. Williams: *Newtonian potential in quantum Regge gravity*, Nucl. Phys. B **435** (1995) 361-398 [hep-th/9406163].
46. I. Khavkine, R. Loll and P. Reska: *Coupling a point-like mass to quantum gravity with causal dynamical triangulations* [arXiv:1002.4618, gr-qc].